NAME OF AUTHOR/*NOM DE L'AUTEUR* Joseph Panno

TITLE OF THESIS/*TITRE DE LA THÈSE* Computer analysis of age-related chromatin condensation in the somatic cells of the housefly Musca domestica

UNIVERSITY/*UNIVERSITÉ* Simon Fraser University

DEGREE FOR WHICH THESIS WAS PRESENTED/*GRADE POUR LEQUEL CETTE THÈSE FUT PRÉSENTÉE* Master of Science

YEAR THIS DEGREE CONFERRED/*ANNÉE D'OBTENTION DE CE GRADE* 1984

NAME OF SUPERVISOR/*NOM DU DIRECTEUR DE THÈSE* Dr. K.K. Nair

DATED/*DATÉ* Dec 27, 1984 SIGNED/*SIGNÉ*

PERMANENT ADDRESS/*RÉSIDENCE FIXE* [redacted]

COMPUTER ANALYSIS OF AGE-RELATED CHROMATIN CONDENSATION IN THE SOMATIC CELLS OF THE HOUSEFLY, MUSCA DOMESTICA

by

Joseph Peter Panno

B.Sc., Simon Fraser University, 1978

THESIS SUBMITTED IN PARTIAL FULFILLMENT OF

THE REQUIREMENTS FOR THE DEGREE OF

MASTER OF SCIENCE

in the Department

of

Biological Sciences

SIMON FRASER UNIVERSITY

April, 1984

APPROVAL

NAME: Joseph Panno

DEGREE: M.Sc.

TITLE OF THESIS: Computer analysis of age-related chromatin condensation in the somatic cells of the housefly Musca domestica

EXAMINING COMMITTEE:

Chairman: Dr. P.C. Oloffs

Dr. K.K. Nair, Senior Supervisor

Dr. B.A. McKeown

Dr. M.J. Smith

Dr. P. Belton, External Examiner

Date approved April 18, 1984

PARTIAL COPYRIGHT LICENSE

I hereby grant to Simon Fraser University the right to lend my thesis, project or extended essay (the title of which is shown below) to users of the Simon Fraser University Library, and to make partial or single copies only for such users or in response to a request from the library of any other university, or other educational institution, on its own behalf or for one of its users. I further agree that permission for multiple copying of this work for scholarly purposes may be granted by me or the Dean of Graduate Studies. It is understood that copying or publication of this work for financial gain shall not be allowed without my written permission.

Title of Thesis/Project/Extended Essay

Computer analysis of age-related chromatin condensation in the somatic cells of the housefly Musca domestica

Author:

(signature)

Joseph Panno

(name)

April 27, 1984

(date)

ABSTRACT

This study was undertaken to assess the degree to which cell nuclei change with age, based on the condensation state and distribution pattern of the chromatin.

Nuclei were examined from the adult male housefly, Musca domestica, reared under high and low activity conditions (male mean lifespans: 14 and 41 days, respectively).

Computer analysis of digitized images of Feulgen-stained nuclei from optic lobe Type II neurons, Malpighian tubule and indirect flight muscle, from the high activity group, showed significant age-related changes in chromatin condensation, as defined by low, medium and high density chromatin components (LDC,MDC,HDC). The relative proportion of each component was found to be both tissue and age-specific. No evidence was found for an age-related change in total DNA content, or a shift in ploidy class frequencies.

The condensation state of the brain, muscle and tubule nuclei tends to increase with age, although the time course of the condensation event and the distribution of the condensed chromatin are tissue specific. Brain nuclei changed more rapidly than either tubule or muscle nuclei. The amount of HDC increases two fold in the brain nuclei, and four fold in the tubule nuclei. This event is accompanied by a 7 to 10 fold increase in the 2-dimensional symmetry of the HDC distribution pattern. Brain and tubule MDC showed fewer changes with age compared with HDC.

By contrast, HDC did not change with age in the muscle nuclei, whereas the amount of MDC showed a significant (16%) reduction by day 4 (decondensation) followed by a 51% increase between day 4 and day 14. The decondensation event corresponds in time to the period of peak flight activity and flight muscle development.

The type II neuron nuclei from the low activity group showed a significant reduction in the amount of HDC, as compared to the high activity group, and a tendency to retain a 1-day-old HDC distribution pattern.

The results of pattern analysis indicate that the various tissues of the male housefly are aging at different rates and that the lowest condensation state of a nucleus is associated with the highest activity level of a cell.

ACKNOWLEDGEMENTS

I would like to thank Dr. K. K. Nair for introducing me to the world of computer mania and for his invaluable guidance, constant support and encouragement. Thanks are also due to Dr. M.J. Smith and Dr. B.A. McKeown for their critical review of the manuscript and for their advice and counsel. I would also like to thank Doug Wilson for the many discussions we have had concerning the theoretical aspects of pattern analysis, Akbar Syed and Marcellino Horta for all the help they gave me in obtaining houseflies, and finally, I would like to thank Diana for her excellent darkroom techniques.

TABLE OF CONTENTS

LIST OF TABLES

LIST OF FIGURES

INTRODUCTION

The development of multicellular organisms can usually be divided into three stages characterized as cellular differentiation and embryogenesis, growth and maturation, and finally senescence. The study of the final stage is referred to as gerontology.

A common view among gerontologists (Hothschild,1971; Sohal,1981; Miquel et al.,1983) is that senescence is the consequence of an error process or the accumulation of potentially toxic compounds, or both. The error process was first proposed by Orgel (1963) and suggests that an error catastrophe might occur if mistakes were made during translation, particularly if the errors involved proteins making up the translation machinery such as ribosomal proteins or tRNA synthetase. Over time the accumulation of such errors would induce senescent changes leading to the death of the organism.

However, Edelman and Gallant (1977) artificially elevated the error frequency nearly 50 times in E. coli without any detectable effect on the mortality rate. In addition, Lamb (1977) elevated the error frequency in Drosophila by including amino acid analogs in their diet without an observable effect on their lifespan. Apparently organisms are capable of preventing an error catastrophe from occuring by degrading abnormal proteins much more rapidly than those that were translated correctly (Goldberg and Dice, 1974).

The accumulation of potentially toxic compounds generally involves an age-related increase in the amount of lipofuscin or the generation of lipid peroxides. The accumulation of lipofuscin is thought to be irreversible and it is believed that its presence in some way interferes with normal cellular activities (Hothschild, 1971; Finch, 1976). However, the lack of experimental evidence in support of this belief is quite pronounced. On the other hand, Davies and Fotheringham (1981) have shown that the age-related increase of lipofuscin in the supraoptic and paraventricular nuclei of the hypothalamus does not limit the production of neurosecretory granules, which is the main function of these cells.

The generation of lipid peroxides has been described in detail by Leibovitz and Siegel (1980). Lipid peroxidation is induced by free radicals produced during normal mitochondrial respiration. These radicals are produced as a consequence of the initial formation of the super oxide radical (SOR) which is formed from molecular oxygen by the addition of a single electron. SOR is acted upon by superoxide dismutase (SOD) to produce hydrogen peroxide, which can then react with SOR to produce the even more potent hydroxy radical (HR). Secondary radicals, such as lipid or purine radicals, are also produced by SOR or HR acting on various biological molecules. The abstraction of an electron and proton from a lipid peroxy radical ultimately leads to the production of lipid peroxides. The significance of lipid peroxides, with respect to cellular

senescence, is that they decompose to aldehydes which cross-link proteins, lipids and nucleic acids (Fleming, et al., 1982).

Antioxidants such as butylated hydroxy toluene (BHT) have been included in the diets of mice to minimize the production of SOR, with a subsequent increase in the mean lifespan of about 45% (Harman, 1968). However, it is not clear if this was due to free radical quenching or if the BHT adversely affected appetite, causing the mice to eat less. This is an important consideration since reduced food consumption can also increase mean lifespan (reviewed in Finch, 1976). A similar study, employing Vitamin C as the antioxidant, had no effect on mean lifespan (Davies, et al., 1977).

The lack of experimental evidence in support of error or toxin accumulation theories has stimulated an interest in models which are primarily concerned with age-related changes at the organismic level. Such models recognize the fundamental nature of the aging process as being due to a highly integrated senescence program at the cellular level and not due to some unfortunate error or waste buildup. In this regard several authors (see review by Everitt, 1980) have proposed models involving an age related breakdown of the interaction between the hypothalamus and the endocrine system in mammals. These models are generally referred to as the Hypothalamic Elevation or Disregulation theories. These theories suggest that the aging of the organism as a whole begins with the senescence of the hypothalamus. Intrinsic aging of the hypothalamus decreases its

sensitivity to feedback inhibition or stimulation by circulating hormones. A notable consequence of this altered threshold in mammalian females is the loss of the reproductive cycle, typically in the second or third quarter of the lifespan.

Transplantation experiments have been performed to test the possibility that the pituitary gland or the ovaries may be responsible for initiating the onset of menopause. Pecile et al. (1966) were able to show that post-reproductive female pituitary glands are capable of supporting postnatal growth and development when transplanted into a young host. Peng and Huang (1972) have shown that the ovaries from old rats (16+ months) regain their estrus cycle (as monitored by vaginal smears) if implanted into young hosts (2-7 months). When prepubertal ovaries were transplanted to old female rats more than 80% of the young ovaries failed to regain their cycles even though the control transplants (young ovaries to young hosts) were more than 85% successful. They were also able to show that some old rat pituitaries (18+ months) were capable of supporting ovarian cycles in young hosts.

On the other hand, several studies concerning the neurotransmitters Dopamine and norepinephrine have shown significant age-related changes in the mammalian brain. Dopamine and norepinephrine are both synthesized from tyrosine via the rate limiting enzyme tyrosine hydroxylase. Finch (1973) and Jonec and Finch (1975) have observed significant reductions in the amount and uptake (by synaptic membranes) of Dopamine in the

hypothalamus and striatum of aging mice. They also observed a reduction in the turnover of hypothalamic norepinephrine. Algeri et al. (1983) found a significant reduction in the conversion of tyrosine to Dopamine and norepinephrine in the hypothalamus of senescent rats and they noted a regional specificity in the age-related decline in tyrosine hydroxylase activity. This latter observation had previously been noted by McGeer and McGeer (1981) in human brain, where a significant decrease in tyrosine hydroxylase activity occurs in 6 areas of the brain while 11 other areas showed no change with age. These results are consistent with the aging hierarchy implied by the hypothalamic elevation or disregulation theories and suggest that the various tissues of an organisim may not age uniformley. That is, an organism may represent a mosaic with respect to the rate at which its various tissue and cell types age.

However, transplantation and neurotransmitter studies have not provided direct evidence for an aging mosaic at the cellular level. Monitoring the cell nucleus over time by analyzing the interphase condensation pattern is one way that this could be done. This would not only provide an estimate of the rate at which the nucleus is changing but would also provide a general estimate of cellular activity. This latter estimate is based on the studies of Harris (1967) involving the reactivation of avian red blood cell nuclei and the subsequent effects on the condensation state of the chromatin, and on several studies which have demonstrated an inverse relationship between the

condensation state of chromatin and its activity level (Littau et al., 1964; Ashburner, 1972; Daneholt, 1975; Lamb and Daneholt, 1979).

Kornberg (1974) and Felsenfeld (1978) have summarized much of what is currently known about the organization of chromatin. The basic subunit of chromatin is the nucleosome, which consists of 2 each of 4 histones (H2A, H2B, H3, H4). Between 140 to 200 base pair (bp) of DNA is associated with each nucleosome. The section of DNA connecting one nucleosome to the other is referred to as the linker. The linker is associated with a fifth histone (H1), which is believed to play an important role in chromosome formation during the cell cycle (Renz et al., 1977). Chromatin also contains many non-histone chromatin (NHC) proteins many of which are believed to be involved in the control of gene expression (Spelsberg et al., 1976) and the maintenance of chromosome structure (McKeon et al., 1984).

Interphase chromatin, though existing in a variety of condensation states, is divided into two broad catagories which are characterized by a low density or diffuse component (euchromatin) and a high density component, referred to as heterochromatin (Hsu, 1962; Brown, 1966). Heterochromatin is further divided into constitutive and facultative forms. Constitutive heterochromatin generally consists of highly repetitive DNA sequences, is non-coding and is usually found in the centromeric regions of chromosomes. Facultative heterochromatin, however, is formed by the condensation of

euchromatin during development. It is known for instance that the deactivation of one of the X chromosomes in human and rat females is accomplished by maintaining the chromosome in a highly condensed state during interphase. This process is referred to as heterochromatinization (Lyon, 1974).

Since it is difficult to distinguish between constitutive and facultative heterochromatin at the light microscope level these two types of chromatin are referred to simply as condensed chromatin (Littau et al., 1965; Kiefer et al., 1973). Euchromatin is generally found to be transcriptionally active, while the activity of condensed chromatin is either nonexistent or greatly reduced (Frenster et al., 1963; Littau et al., 1964; Panar and Nair, 1975; Maclean and Hilder, 1977). The correspondence between the structural conformation of chromatin and transcriptional activity has also been demonstrated through ultrastructural studies (Daneholt, 1975; Lamb and Daneholt, 1979; Hamkalo and Rattner, 1980) and DNAase I digestion studies (Weintraub and Groudine, 1976).

Condensation of chromatin has been observed during the differentiation of insect flight muscle (Panar and Nair, 1975), during the maturation of mammalian erythrocytes (Gersh,1973), and during programmed cell death or apoptosis (Wyllie et al., 1981).

Chromatin condensation also appears to be associated with the aging process. Phytila and Sherman (1968) and von Hahn (1970) demonstrated an age-related increase in the thermal

stability of chromatin when 1 to 3% residual histone was left intact. Purified DNA showed no such trend. Subsequently, O'Meara and Hermmann (1972) have shown that chromatin from the liver of old mice is more resistant to salt dissociation than liver chromatin from young mice. Transcriptional activity was shown to decrease over the same time period. However, biochemical studies such as these are unable to provide information on specific cell types. In addition, the comparisons are usually restricted to two age groups without any regard for the time course of the event.

Fankboner (1978), using microspectrophotometry, attempted to show an age-related increase in the condensation state of nuclei from a single cell type in mid-gut epithelium from the desert locust, Shistocerca gregaria. However, it was not clear from this study whether the observed change was due to maturation or to aging. In addition, nuclei were examined from only two age groups. Ultrastructural studies of neurons from the brain of Drosophila (Miquel, 1971) and from the optic lobes of the scorpion fly, Panorpa vulgaris (Collatz and Collatz, 1981) have shown a general increase in the condensation state of the nuclei, in parallel with a decrease in both nuclear and cell area. No attempt was made to examine the condensation state of different cell types and in the case of Miquel (1971) only two age groups were examined.

The purpose of this study was to examine the condensation state of three tissue types from several age groups in an

attempt to answer two basic questions. First; does the condensation state of cell nuclei change with age and second; if it does, is there any indication that the change is tissue specific with respect to both the pattern and the time course of the event. To this end I have used computer assisted Feulgen-microspectrophotometry, whereby a digital image of a cell nucleus is generated which can be subjected to pattern analysis after the methods of Wied et al. (1968), Vidal et al. (1973), and Sherwood et al. (1976).

The male housefly was chosen for this study for three main reasons. First; all of the adult tissues, with the exception of the germ line, are post-mitotic (Clark and Rockstein, 1964). Second; it is known that the male housefly is fully mature 1 day after adult emergence (Rockstein and Bhatnagar, 1966; Clark and Rockstein, 1964), and third; the adult male has a relatively short mean lifespan which can be varied from 2 weeks, when reared under high activity conditions, to 5-6 weeks when reared in isolation (Sohal and Donato, 1978).

MATERIALS AND METHODS

Histology

Preliminary histological preparations of the brain and the Malpighian tubules were done in order to facilitate preparation of the tissues for microspectrophotometry.

A cross section of the brain, stained with Schiff's reagent and counter-stained with Fast Green, is shown in Fig. 1. This section is viewed from the anterior and is approximately midway through the brain. The brain consists of two relatively large optic lobes (OL) at either end of the pars intercerebralis (PI). The neurons used in this study are type II neurons from the optic lobes. These neurons have a diameter of 3 to 5 μm, are monopolar and have very little cytoplasm (Sohal et al., 1972). They also account for nearly 60% of all neurons in the optic lobe. Large clusters of type II neurons are indicated by the solid arrows in Fig. 1. An electron micrograph of a single type II neuron is shown in Fig. 2.

Malpighian tubules in the housefly occur as two pairs of tubules arising on either side of the gut and are attached by a single duct which joins the gut at the ventricular-pyloric junction. One pair occupies the anterior region of the abdomen while the second pair occupies the posterior region (Fig. 3). The anterior and posterior tubules are about 0.1 mm in diameter with the anterior tubule being longer with a total length

Figure 1. Crossection of the brain from a 1-day-old adult male, M. domestica.

The section is an anterior view, midway through the brain, showing the pars intercerebralis (PI), optic lobes (OL) and a part of the ommatidia. Clusters of type II neurons are indicated by the arrows. The tissue was fixed in 10% buffered formalin (pH 7.2) for 1h, stained with Schiff's reagent for 1h, dehydrated and embedded in paraplast (paraffin wax). Sections were cut at 5.0 µm, mounted on albumunized slides, dewaxed, hydrated and counter-stained for 1 minute with 0.5% Fast Green, after which the sections were dehyrated, cleared in xylene and mounted in Permount. (Mag. 130X).

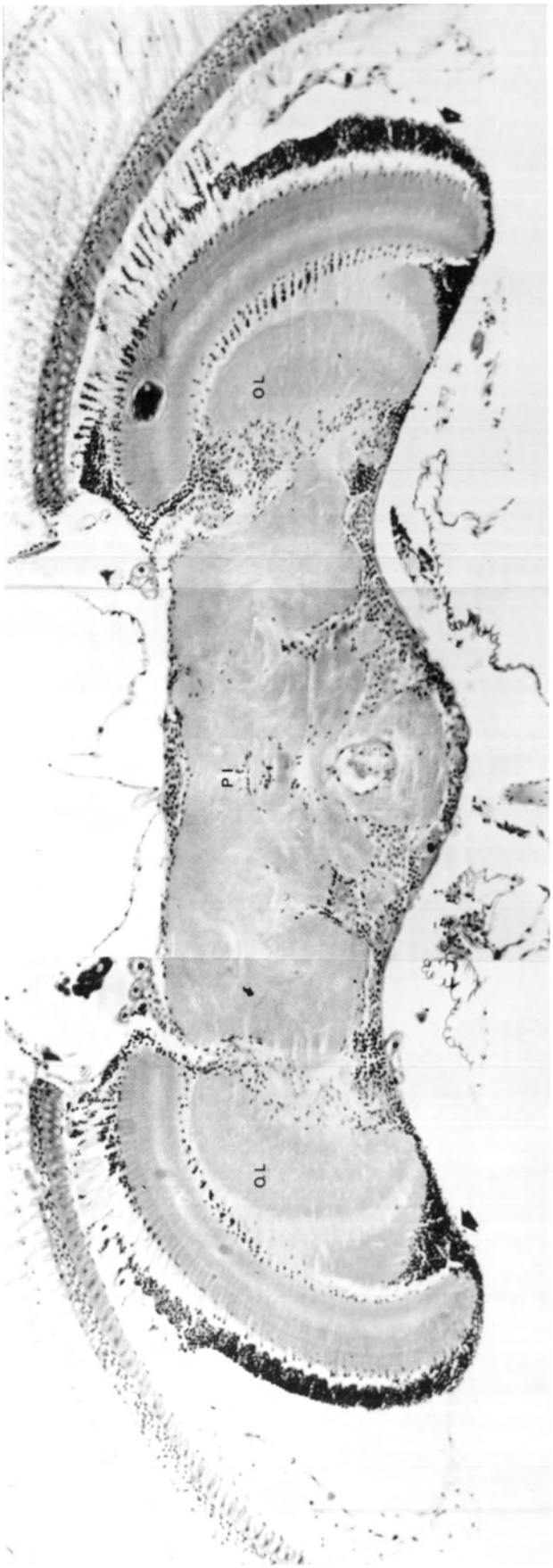
TO
PI
TO

Figure 2. Electron micrograph of a type II neuron from the optic lobe of a 1-day-old adult male, M. domestica.

Nucleus (N), cell membrane (solid arrow). Isolated brains were fixed for 2h in Karnovsky's fixative (25% formaldehyde, 25% glutaraldehyde, 0.2 M sodium cacodylate, 4.6 mM $CaCl_2$), post-fixed in 0.1% OsO_4 in 0.1 M cacodylate buffer (pH 7.2) for 2 hours at $4^{o}C$. The tissue was embedded in Spurr expoxy media and sections stained with Reynolds' lead hydroxide-citrate (45% w/v Lead Nitrate, 5.9% w/v sodium citrate) and counter-stained with saturated uranyl acetate in 50% Ethyl Alcohol. (Mag. 18,500X).

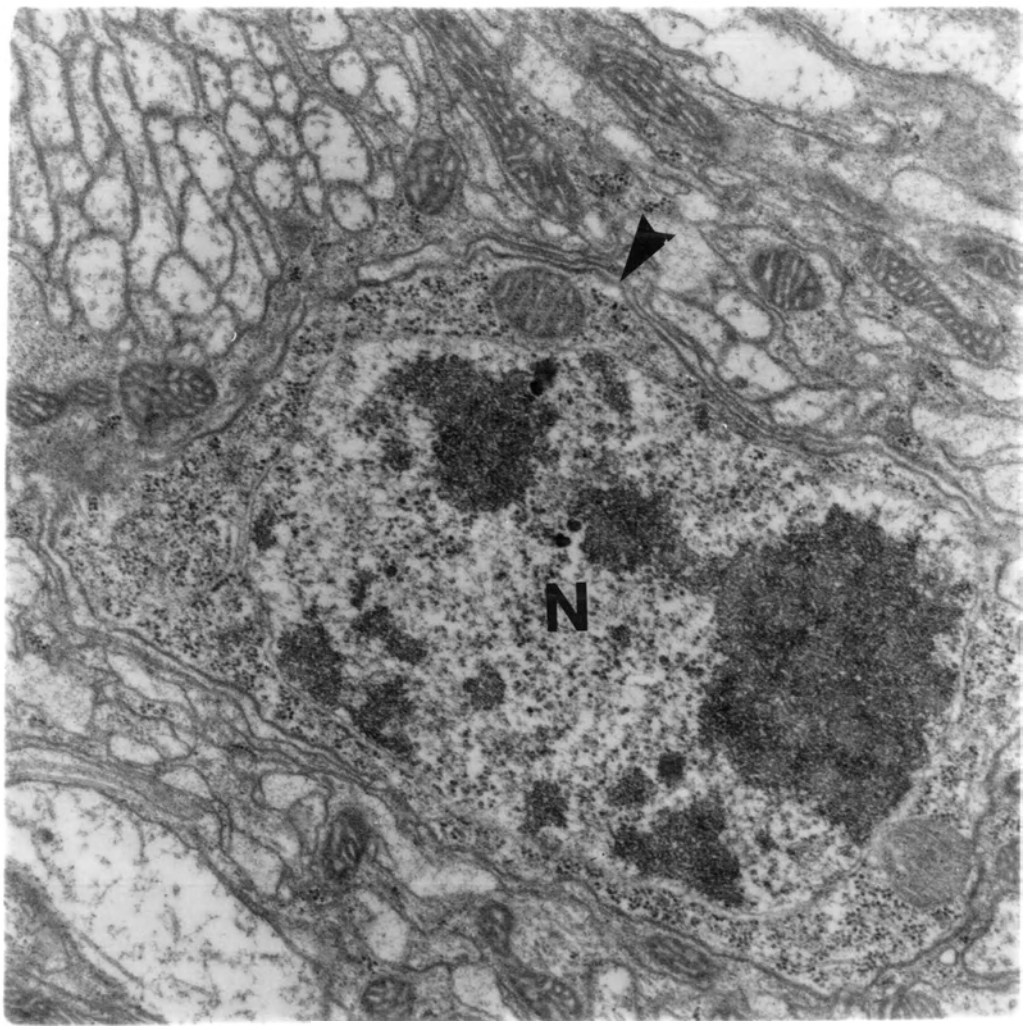
N

Figure 3. Diagramatic sketch of the Malpighian tubules from the adult, M. domestica, indicating the point of origin at the ventricular (V) pyloric (P) junction. Anterior is towards the top of the page. (Mag. 50X).

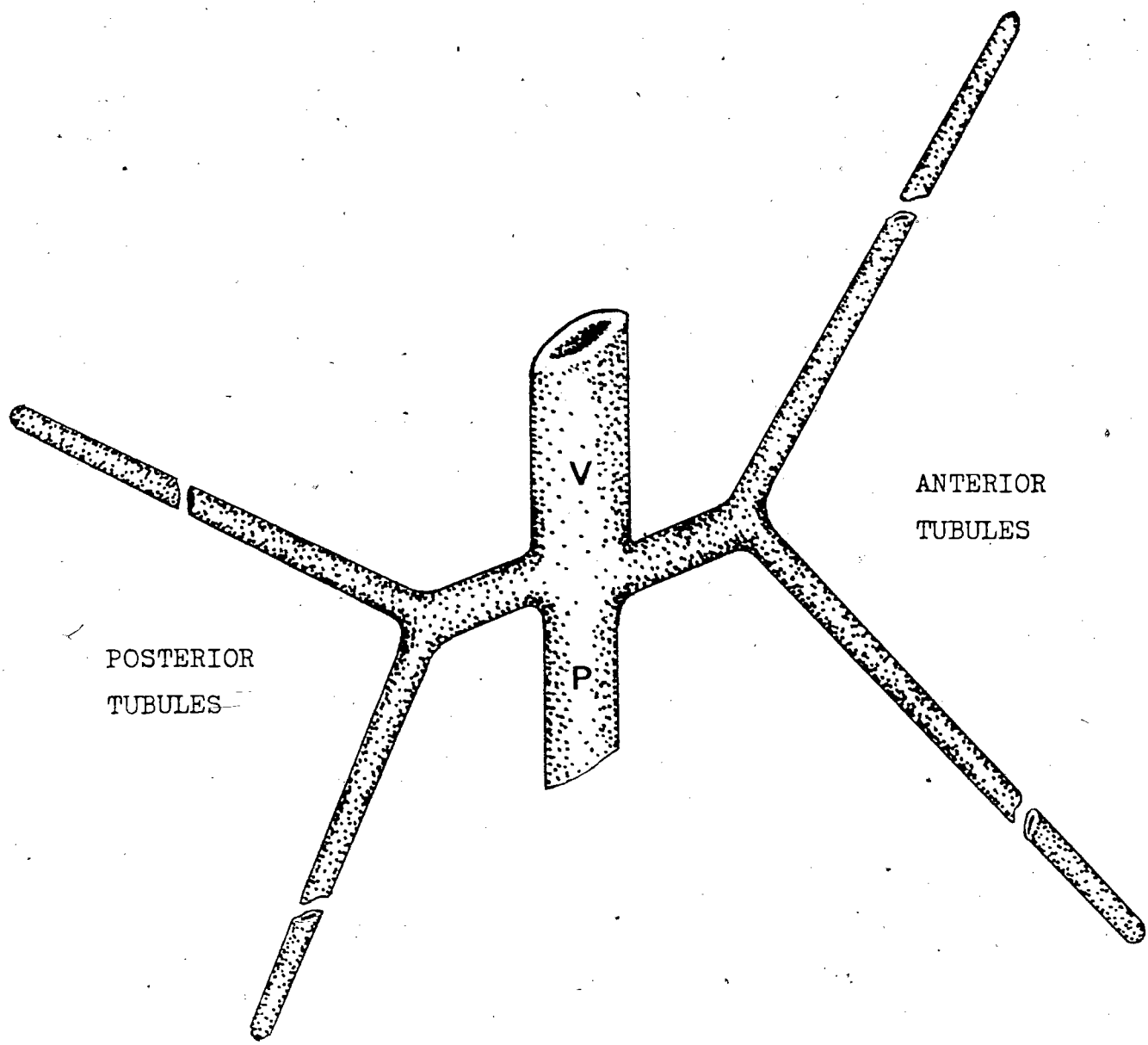
V
P
ANTERIOR
TUBULES
POSTERIOR
TUBULES

(both arms) of about 22 mm as compared to 13 mm for the posterior pair. The extra length of the anterior pair is due in part to a bladder like section at the distal tips, the exact function of which is unknown (Miller, 1965). The posterior tubules alone were used in this study. The tubule wall is one cell thick, and is constructed by the helical opposition of two cells (Fig. 4A). A cross-section of the tube shows that the large nuclei have a flattened profile on the surface facing the lumen of the tubule (Fig. 4B). The plano-convex profile of this nucleus appears to be a common characteristic of Malpighian tubule nuclei in Drosophila (Miller, 1965) and Rodnius (Wigglesworth, 1972).

Rearing

Adult houseflies were reared according to Rockstein and Lieberman (1959) on milk powder, sugar and water in 3.1 liter nylon mesh cages. The colonies were maintained in an incubator at 27°C, 40% relative humidity and a 15h photoperiod. These males constitute the high activity (HA) group. Tissues processed from this group included brain, Malpighian tubules and flight muscle.

A second group of male houseflies was reared individually in small (340 cc) nylon mesh cages at the same temperature and relative humidity as the HA-group and they constitute the low activity (LA) group.

Figure 4. Micrographs of Malpighian tubules from 1-day-old adult male, M. domestica.
(A) Whole mount, (B) cross-section showing the profile of a tubule nucleus.
A: Isolated tubules were fixed in 10% buffered formalin (pH 7.2) for 1h, stained with Schiff's reagent for 1h and counterstained in 0.5% Fast Green for 1 min., followed by deydration, clearing in xylene and mounting in Permount. (Mag. 225X).
B: Whole abdomen was fixed, stained with Schiffs' reagent as in (A), dehydrated and embedded in Paraplast (embedding wax). Sections were cut at 5.0 µm, mounted on albuminized slides, dewaxed, hydrated and counter-stained with 0.1% Eosin, dehydrated, cleared in xylene and mounted in Permount. (Mag. 1480X).

A

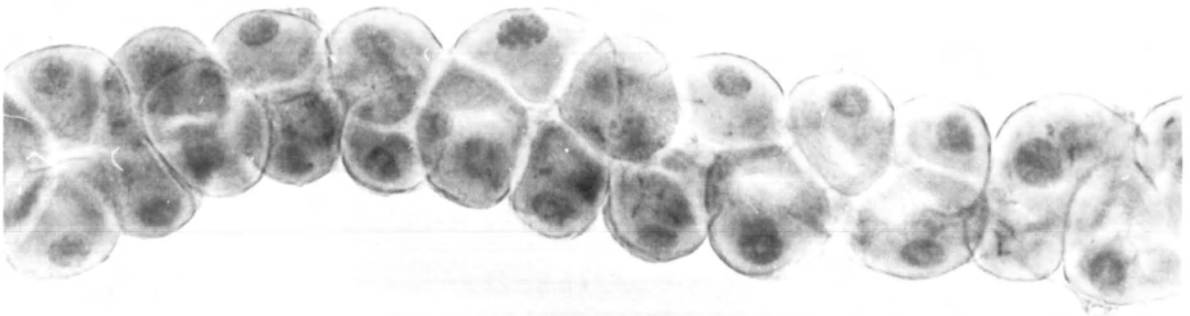

B

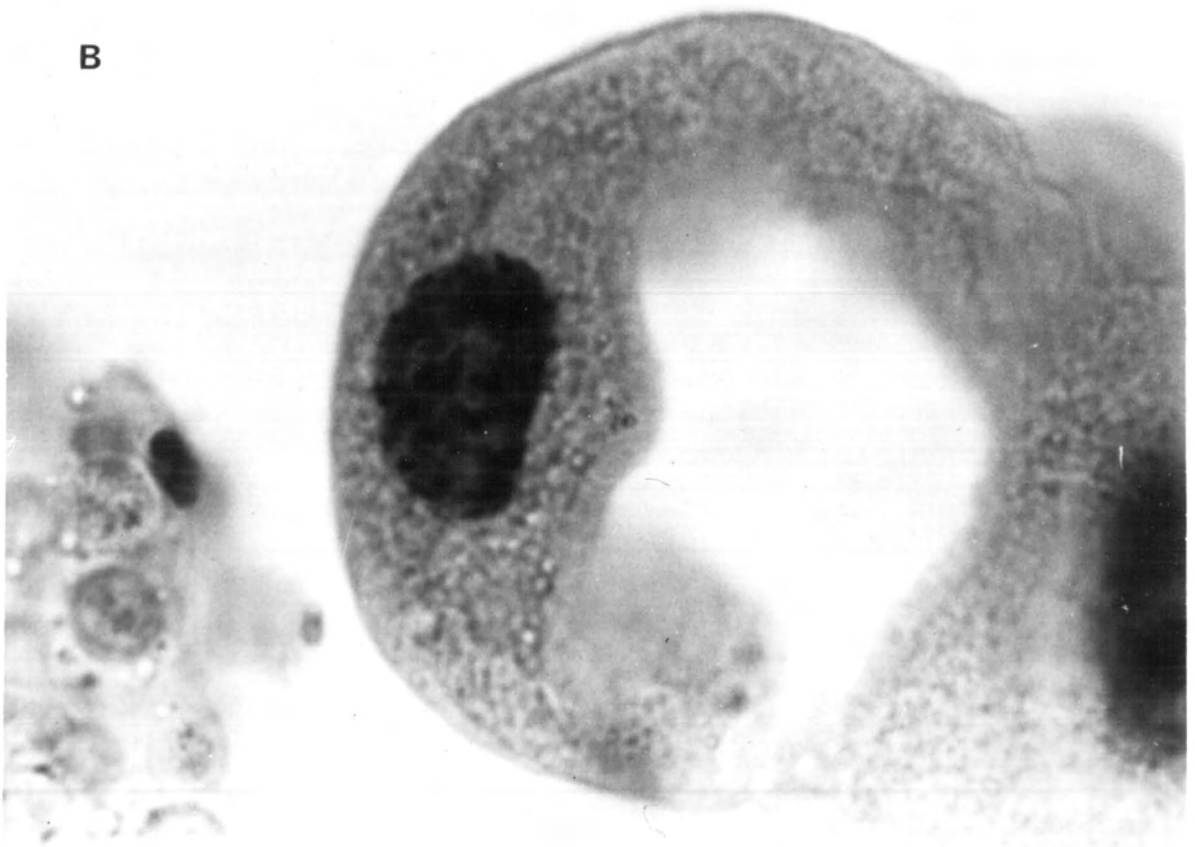

Tissue Preparation

Adult HA-males were collected, anesthetised very briefly with CO_2, and then decapitated. The heads, abdomens and thoraces were fixed in bulk in buffered 10% formalin (pH 7.0) for 2h after which the tissues were washed for 2h in distilled water and then stored in 70% ETOH. Further processing occurred after all tissues from each age group had been collected. This involved acid hydrolysis in 3.5N HCl for 30 minutes, as this was determined to be the optimal hydrolysis time, at 37°C (Fand, 1972), followed by staining in fresh Schiff's reagent (Basic Fuchsin,Harleco) for 1h in the dark. The bulk-stained brain, Malpighian tubules and muscle were dissected out and cleaned of fat body and trachea. The separated optic lobes, Malpighian tubules and muscle tissue were squashed on gelatinized glass slides (coverslips were removed by the dry ice method), dehydrated, cleared and mounted in oil of matching refractive index (nD = 1.56, Cargille). Optic lobe and flight muscle tissue was obtained from 5 individuals per age group, whereas tubules were obtained from 4 individuals per age group. Nuclei from the brain were examined from 7 age groups (4-hour, 1-day, 2-day, 3-day, 4-day, 8-day and 14-day), while nuclei from the tubules and flight muscle were examined from four age groups (1-day, 4-day, 8-day and 14-day). Age groups beyond 14 days have not been included to avoid problems of cross-sectional sampling

(Sohal and Donato, 1978). The age of each group was known to within four hours. Squashes were also prepared from Feulgen-stained testis to establish the ploidy levels of the brain, tubule and muscle nuclei. The nuclei measured in the brain were from Type II optic lobe neurons (described above). All reference to brain nuclei will be understood to mean this neuron exclusively. In the tubules, nuclei of all classes present were measured at random. A total of 150 nuclei was measured from the brain and 100 from the tubules for each age group, whereas 50 nuclei per age group were measured in the flight muscle.

Optic lobe squashes were prepared from the LA-males as described above. Malpighian tubules and flight muscle were not processed. 75 nuclei, from type II neurons, from 3 individuals were measured per age group. All reference to tissues from the high activity group will be simply brain, tubule or muscle.

Microspectrophotometry

All measurements were obtained with the Scanning Microscope Photometer(SMP. Carl Zeiss) which is on line with PDP-12 and IBM-3033 computers. The diameter of the measuring aperture was 0.5 µm. The Feulgen-stained nuclei were scanned at 575 nm using a step size of 0.5 µm. In all cases, the age of the tissue was unknown while the slides were being scanned.

A fundamental problem in chromatin pattern analysis is that of selecting a suitable optical density (O.D.) that will serve as a boundary separating noncondensed chromatin (NCC) from condensed chromatin (CC). Although some authors have adopted a single boundary solution (Vidal et al., 1973; Sherwood et al., 1976; Mello, 1978) I have not found it to be entirely satisfactory and instead adopted the following procedure.

An initial boundary (IBND) separating NCC from CC was calculated by the method of Vidal et al. (1973) using nuclei from the 1-day-old group for each tissue type. Next, the average maximum optical density (ODMAX) was obtained for each cell and ploidy type, and from this a midpoint (ODMID) between IBND and ODMAX was calculated. This procedure generates two major chromatin components; the non-condensed or low density component (LDC) extending from an optical density of 0.02 up to IBND, and a condensed component, extending from IBND to 2.0. The condensed component is further divided into two subcomponents; the Medium Density Component (MDC) extending from IBND to ODMID, and a High Density Component (HDC) extending from ODMID to ODMAX. The location of these components over an optical density range of 0.02 to 2.0 is diagrammed below. ODMAX will always be less than or equal to 2.0.

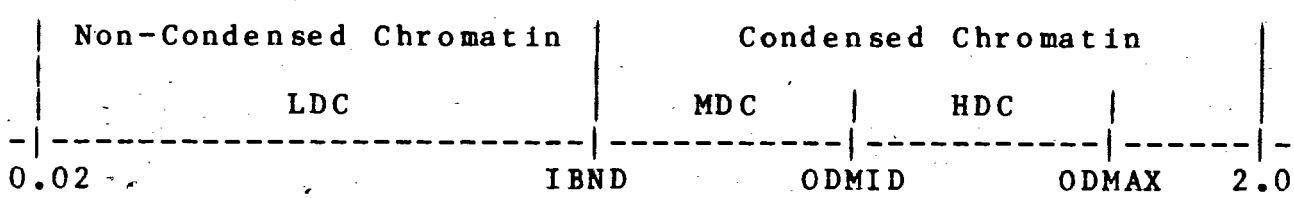

Once these boundaries were established it was possible to extract several image features per component relating to the magnitude and spatial symmetry of the condensation event. In addition, two global features were extracted which are independent of boundary intervals. These features are described briefly below:

1. Global Features:
   a. Total nuclear O.D. The sum of all O.D. values making up the digitized image. This sum is proportional to the total DNA content of the nucleus.
   b. Total nuclear area (TNA). The number of values making up the digitized image.
2. Image Features:
   a. Total O.D. of the High and Medium Density Components (TOHDC, TOMDC). expressed as a percentage of total nuclear DNA.
   b. Total Area occupied by the MDC and HDC (TAMDC, TAHDC), expressed as a percentage of the total nuclear area.
   c. Symmetry Index (SI). An approximately circular nucleus can be divided into four nearly equal quadrants. SI gives a measure of how evenly the condensed chromatin (either MDC or HDC) is distributed over the four quadrants. SI will range from 0 (perfect asymmetry) to 10 (perfect symmetry) and represents an idealized symmetry.
   d. Quadrant Symmetry Index (QSI). This is an estimate of

the actual number of quadrants being occupied by MDC or HDC.

e. The Number of Condensed Chromatin Clusters (NOC). Refers to one or more O.D. values in the HDC or MDC range which are surrounded by another component.

f. Cluster Distance Index (CDI). This estimates the average distance of MDC or HDC clusters from the geometric center of the nucleus and expresses it as a percentage of the nuclear radius.

Data Analysis

Comparisons between the different age groups based on the image features were analyzed for significance using the nonparametric Kruskal-Wallis test (Bartels, 1979).

The features showing the greatest differences were then used in a non-parametric discriminant analysis in order to classify nuclei from various age groups as belonging to either the 1 day or 14 day old groups. Fundamental to this classification is the calculation of an ambiguity function and merit value for each feature over a specified boundary interval (Bartels, 1979). The merit value is calculated from the following expression:

Merit = Dprime + 0.5(1.0 - Ambiguity).

Dprime and Ambiguity are independent estimates of the degree to which the distribution of a 1-day feature overlaps with the distribution of the same feature from the 14-day group. If there

is no overlap in the distributions, Dprime will equal 0.5 and Ambiguity will equal 0. The Merit value will then be equal to 1.0 (Bartels, 1979). The features with the highest merit values are then used to generate a training set by a program called LEARN. The training set is a collection of feature values which serve as decision boundries in a classification procedure. By applying the decision boundries, a nucleus can be assigned to either a 1-day or 14-day group depending on whether the corresponding feature value for that particular nucleus is greater or less than the decision boundary. To illustrate, consider a 1-day and 14-day group and the feature TOHDC (total O.D. of the high density component as a percent of total nuclear DNA). A hypothetical analysis shows that TOHDC accounts for 10% of total DNA in the 1-day group and 30% in the 14-day group. The program LEARN evaluates the frequency distribution of TOHDC for both groups simultaneously and decides that the best decision boundary is a TOHDC of 12%. A decision rule could then be as follows: assign the nucleus to the 14-day group when TOHDC is greater than 12%, otherwise assign it to the 1-day group. The features used in the classification procedure were extracted from the high density component.

RESULTS

The survival curves for the high activity (HA) and low activity (LA) groups are shown in Fig. 5. The HA-males had a mean and maximum lifespan of 14 and 34 days respectively. The mortality of the males at 14 days is 70% increasing to 90% by day 17. The LA-males had a mean and maximum lifespan of 41 and 64 days respectively. This group did not reach 70% mortality until day 46, increasing to 90% at day 60.

One external sign of age in the male housefly is fraying and eventual loss of the wings (Rockstein and Brandt, 1963). 50% of the HA-males were grounded due to the loss of one or both wings by day 6, increasing to 80% by day 8. The LA-males retained both wings until day 10, with 5% losing one or both wings between day 11 and day 14 (Fig. 6.).

Fig. 7 shows the total DNA content (expressed as $\log_2$ of total O.D.) of the brain, muscle and tubule nuclei from 4 age groups. The type II neurons are diploid, since the average O.D. value is double that of the haploid spermatid nuclei, whereas the muscle nuclei are tetraploid. The tubules consist of 4 ploidy classes of 8C, 16C, 64C and 128C nuclei. The shift in the proportions of 64C and 128C nuclei between day 4 and day 14 is probably due to the fact that the male population contains individuals with variable proportions of these two ploidy classes (Table 1).

Sohal (1974) has identified three distinct cell types (I,II,III) making up the tubule and a fourth cell type (type IV)

making up the ducts. The measurements of total O.D. from the tubule nuclei (Fig. 7) indicate that cell types II and IV correspond to an 8C and 16C ploidy class nucleus, while Type I and Type III correspond to 64C and 128C nuclei. The assignment of these ploidy classes is tentative, as Sohal (1974) did not measure DNA content but only refers to general size differences. In addition, I have found four distinct ploidy classes in the tubule (Fig. 7) which could mean that the type II cell has both 8C and 16C nuclei, or that the type IV cell is not restricted to the duct as Sohal (1974) suggests. Considering the rarity of the 16C class in the tubule (see Fig. 7), it is possible that Sohal (1974) could have overlooked it in his ultrastructural studies. The 64C and 128C nuclei range in diameter from 25 to 45 um and the 8C and 16C nuclei are between 10 and 12 um. Three principle cell types can be seen bulging from the tubule in the scanning electron micrograph shown in (Fig. 8).

Sohal (1974) observed a random distribution of cell types I, II and III along the tubule. The distribution of these cells was examined in the present study by recording both the total O.D. and relative position of each nucleus in tubules from two individuals. The position of the 8C and 16C class was recorded in only one of the two arms. The results (Fig. 9A,9B) showed that while there is some tendency for the 64C and 128C nuclei to appear as clusters, they are distributed along the entire length of the tubule.

Figure 5. Survival curves for high activity (●) and low activity (○) adult male, M. domestica. The curve for the high activity group is an average from four colonies representing a total of 1233 adult males. This group was reared in large (3.1 liter) nylon mesh cages with about 300 males and 300 females per cage. The curve for the low activity group is based on 20 adult males, each reared in separate small (340 cc) nylon mesh cages.

The mean lifespans are 14 and 41 days, respectively for the high and low activity group. The means ($\bar{x}$) are calculated from the following expression (Weinburg and Shumaker, 1974):

$$\bar{x} = 0.5 + \sum fx \; / \; N$$

where fx = the number of individuals dying on a given day times the number of days they survived.

and N = total number of individuals in the population.

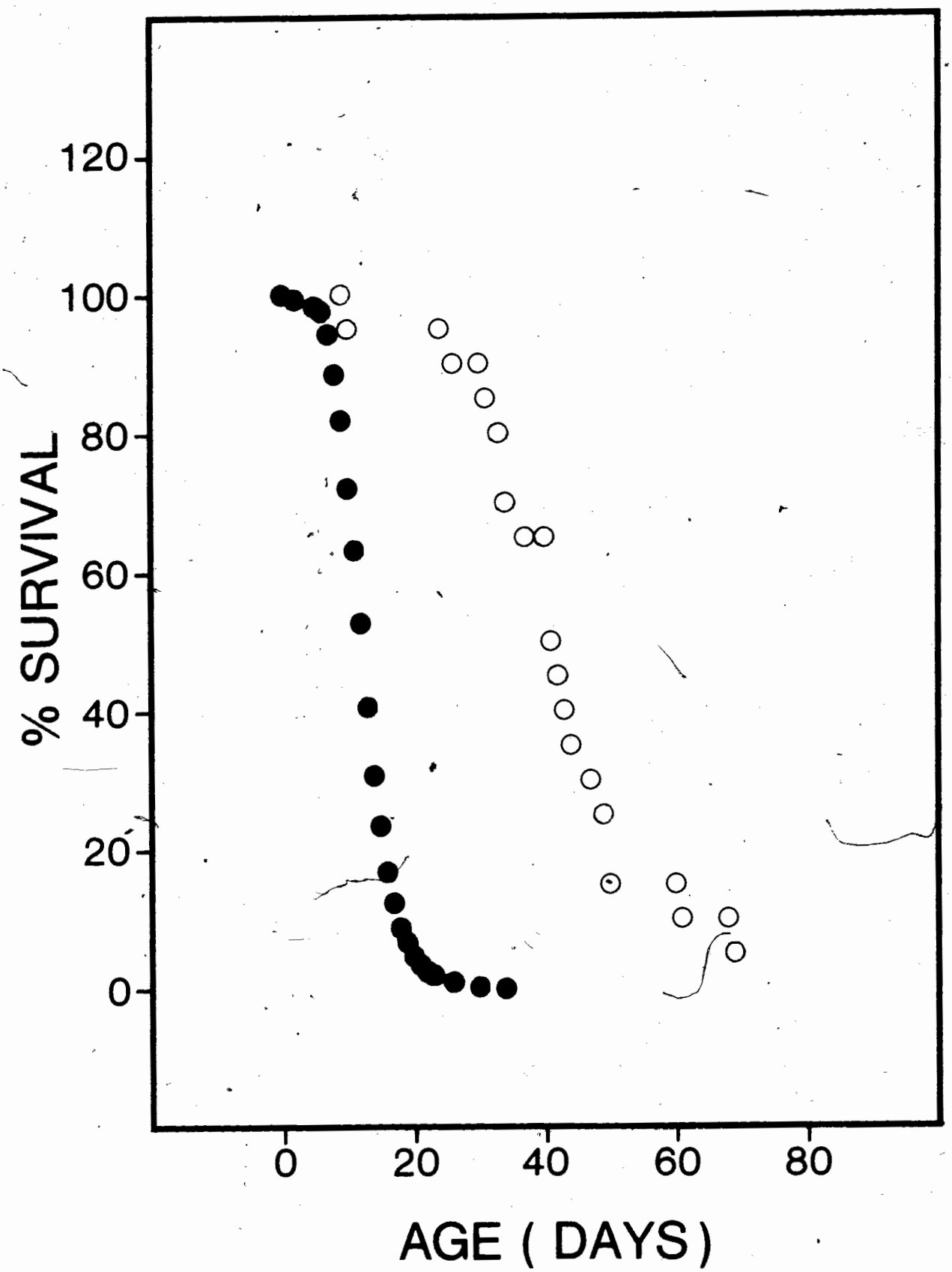
120
100
80
60
40
20
0
% SURVIVAL
0
20
40
60
80
AGE (DAYS)

Figure 6. The percent of adult male, M. domestica that have lost one or both wings with age. The number of individuals scored per day is given in parentheses.

● High activity group (75).

○ Low activity group (20).

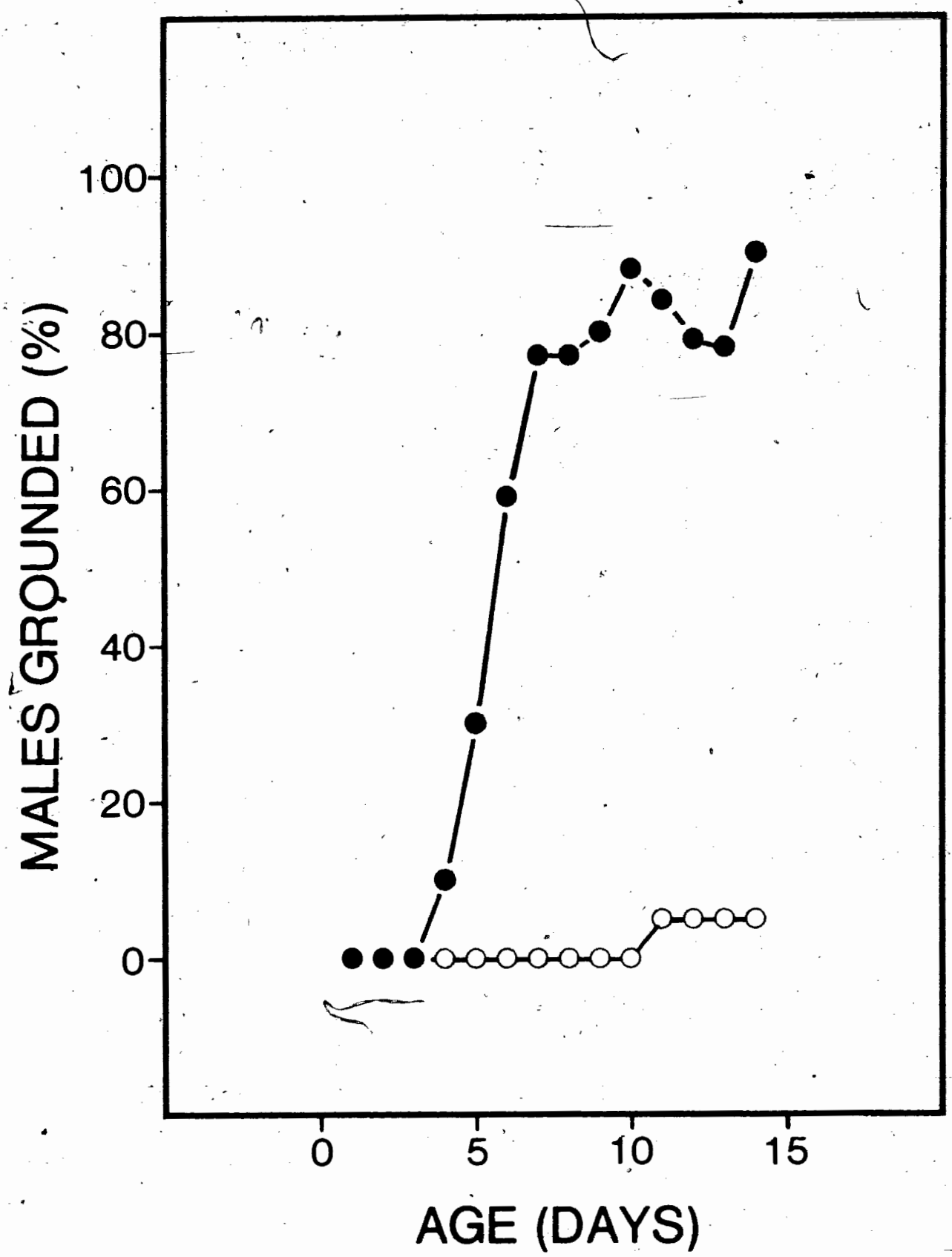
MALES GROUNDED (%)
100
80
60
40
20
0
0
5
10
15
AGE (DAYS)

Figure 7. Frequency distribution of DNA ploidy levels in nuclei of brain (open bar), flight muscle (hatched bar) and Malpighian tubule (solid bar) of adult male, M. domestica, determined by Feulgen-microspectrophotometry. Numbers of nuclei measured for each tissue are given in parentheses. Brain (150), flight muscle (45), tubule (100).

A: 1-day-old

B: 4-day-old

C: 8-day-old

D: 14-day-old

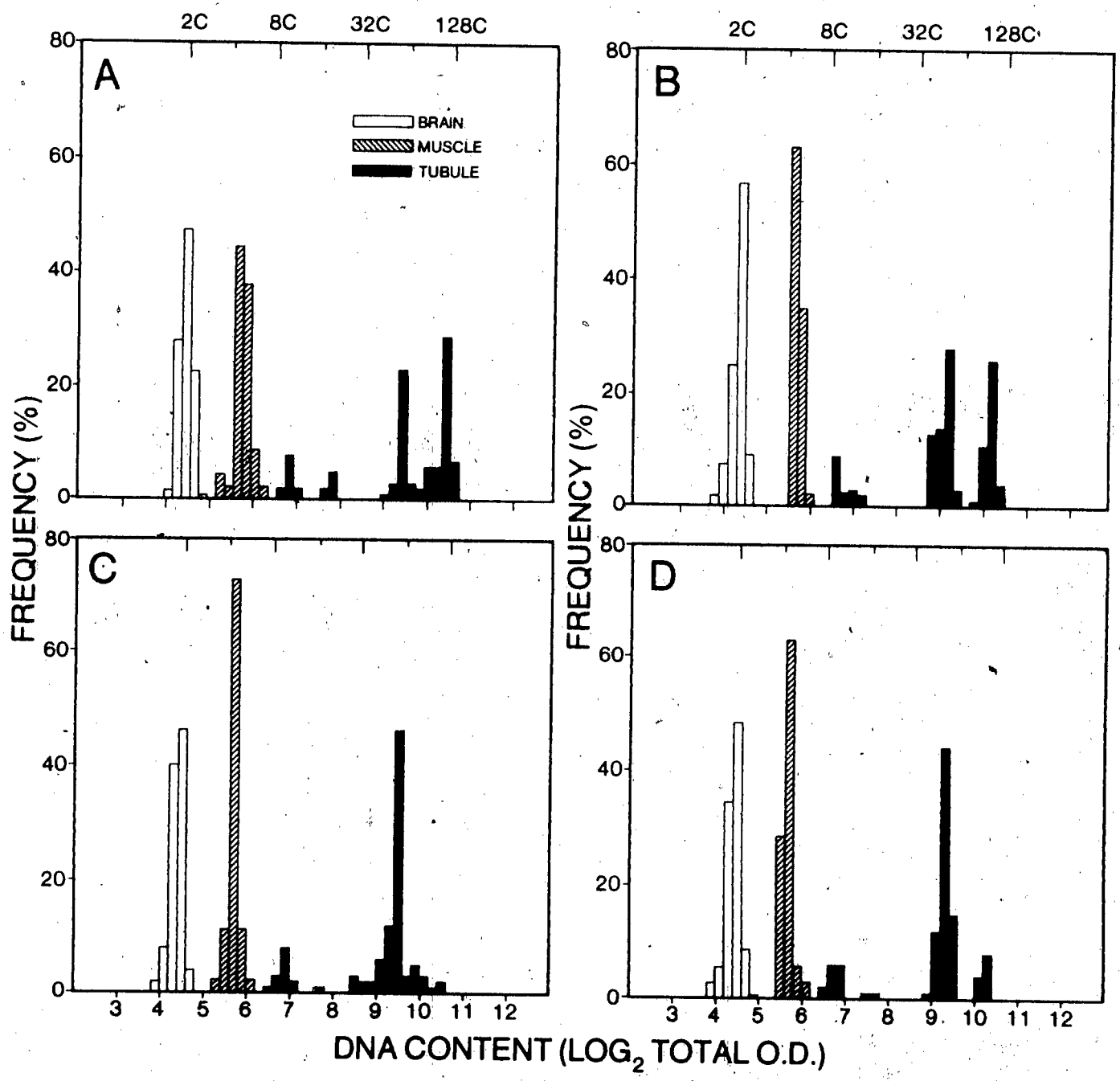
2C
8C
32C
128C
A
B
C
D
BRAIN
MUSCLE
TUBULE
FREQUENCY (%)
0
20
40
60
80
3
4
5
6
7
8
9
10
11
12
DNA CONTENT (LOG2 TOTAL O.D.)

Table 1

The relative proportions of 64C and 128C nuclei present in the Malpighian tubules of high activity adult male, *M. domestica*.

Age (days)	A		B		C		D	
	64C	128C	64C	128C	64C	128C	64C	128C
1	95	5	25	75	32	68	5	95
4	44	56	80	20	28	72	64	36
8	100	0	100	0	90	10	60	40
14	95	5	67	33	95	5	86	14

The table values are percentages of approximately 20 nuclei per individual. Each age group consists of four (A,B,C,D) individuals.

Figure 8. Scanning electron micrograph of a Malpighian tubule from an adult male, M. domestica. The micrograph shows a portion of one pair of tubules (T) attached to the duct (D) and lying over the gut (G). Three principal cell sizes can be seen bulging from the tubule. (Mag. 140X). Whole abdomen was fixed for 1 hour in 10% formalin, dehydrated through an alcohol and amyl acetate series and critical point dried. Arrows indicate the various cell types.

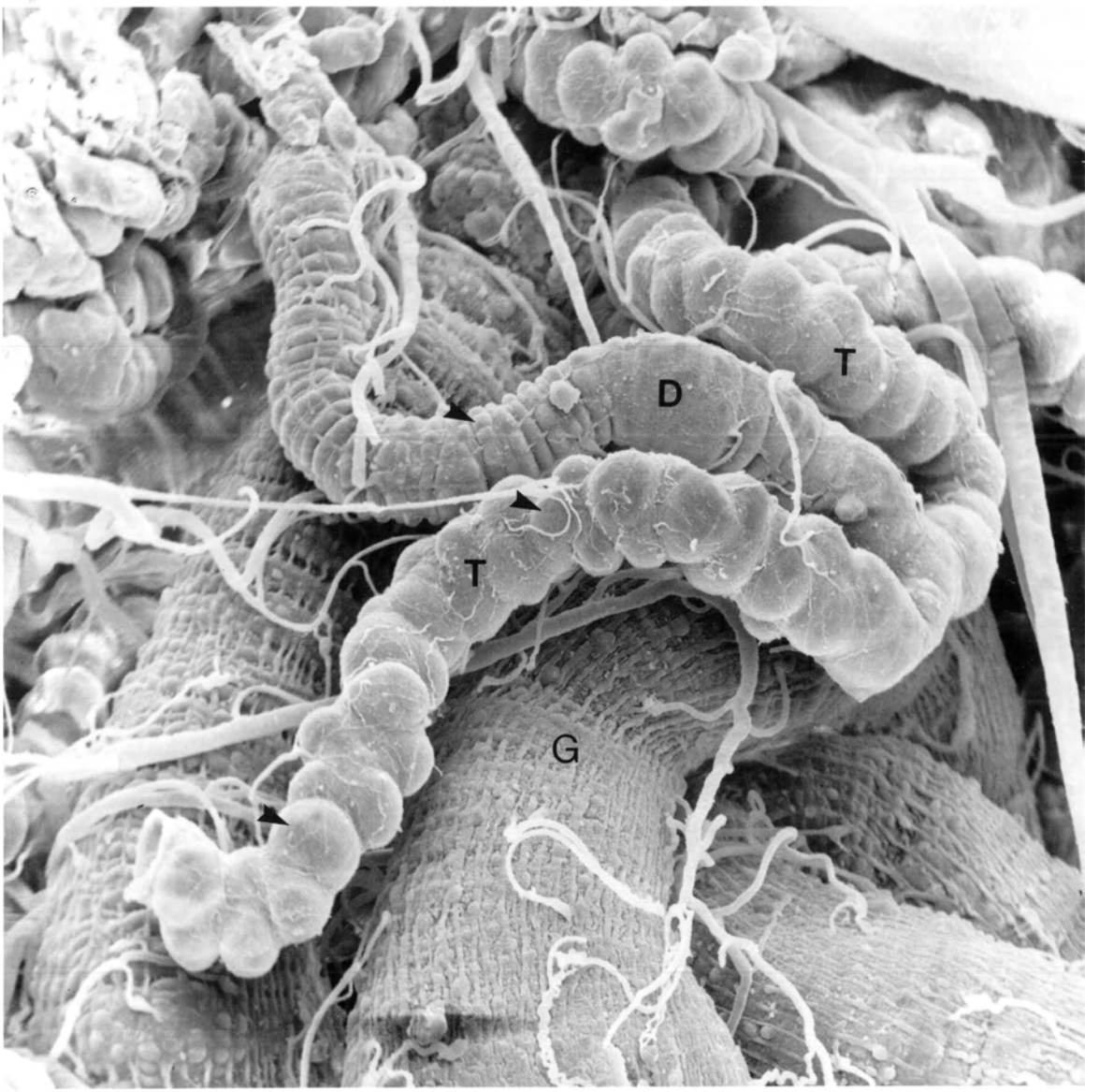
D
T
T
G

Figure 9. Computerized sketch of Malpighian tubules from two (A, B) 1-day-old adult male, M. domestica showing the relative positions of the four ploidy class nuclei.

◇ 8C and 16C nuclei.

○ 64C nuclei.

● 128C nuclei.

⊠ Nuclei that were not measured.

The 8C and 16C nuclei were grouped together due to the rarity of the latter class, and were recorded in only one arm of each tubule. The vertical section indicates the location of the duct.

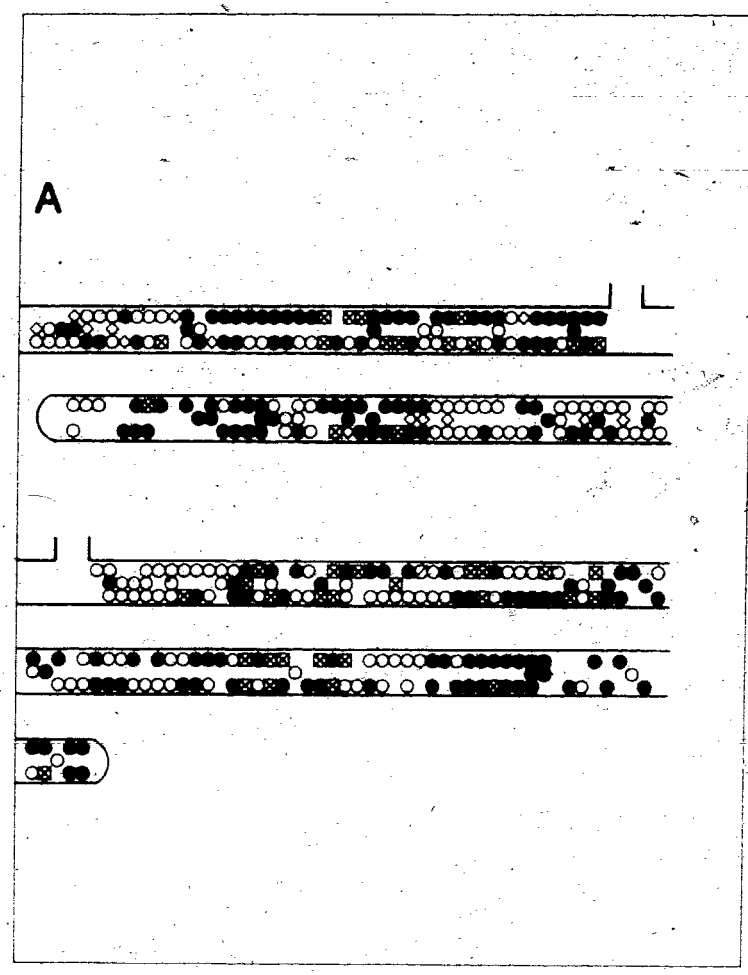
A

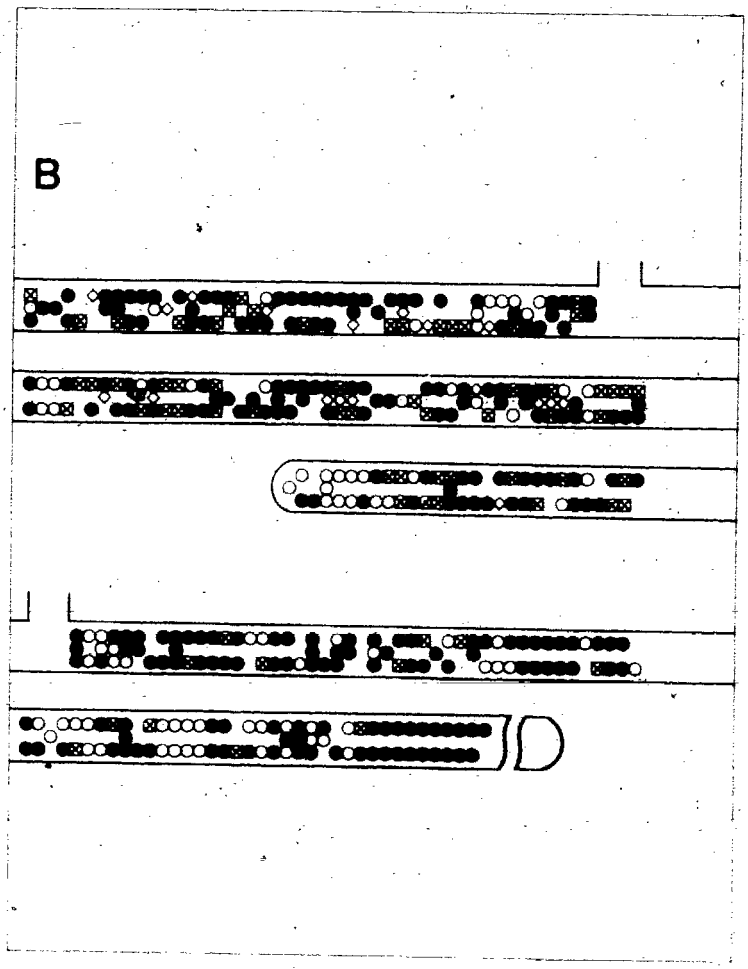
B

Pattern analysis of the tubule nuclei showed significant changes with age in the 64C class but not in the 8C class (Tables 2 and 3). A significant HDC condensation event occurred in the 128C class between day 8 and day 14, with no change between day 1 and day 8. (Table 4). However, since the very large size of these nuclei predisposes them to possible distortion during preparation, no conclusion is being drawn from this event or to any event occuring in the MDC (Table 5). The 16C class was not analyzed due to its rarity (Fig. 7). Therefore, unless the ploidy class is explicitly stated, further reference to tubule nuclei will be understood to mean the 64C class only.

Total O.D. as a function of age in brain, muscle and tubule nuclei is shown in Fig. 10. Total O.D. does not change significantly in the brain ($P > 0.05$), although a slight (10-12%) but significant reduction occurred in the muscle, 8C, 64C and 128C tubule nuclei ($P < 0.05$).

The relative proportions of the LDC, MDC and HDC in the brain nuclei are shown in Fig. 11A. Only 4 age groups are shown in this Figure for clarity. At day 1 the brain nuclei contain approximately 30% LDC, 40% MDC and 27% HDC. These proportions change significantly by day 4 with a reduction in LDC and MDC to 17% and 30% respectively ($P < 0.01$). This is associated with a highly significant increase in HDC to nearly 50% of total DNA ($P < 0.01$). The day 4 proportions remain unchanged through to day 14 ($P > 0.05$).

Table 2

Means and standard deviations (SD) for the medium density component (MDC) of 8C Malpighian tubule nuclei from high activity adult male, M. domestica.

Feature	1 day	8 day	14 day
	Mean ± SD	Mean ± SD	Mean ± SD
TOMDC	37.8 ± 10.2	49.0 ± 21.4	47.6 ± 13.0
TAMDC	26.5 ± 10.5	38.9 ± 20.6	36.6 ± 12.9
CDI	59.6 ± 3.6	55.7 ± 5.4	55.0 ± 3.7
NOC	7.9 ± 4.0	3.3 ± 3.2	4.1 ± 3.5
SI	2.8 ± 1.5	4.8 ± 2.6	4.4 ± 1.8
QSI	3.2 ± 0.5	3.4 ± 0.7	3.3 ± 0.6

Differences between the three age groups, for any feature, is not significant ($P > 0.05$). (TOMDC, TAMDC) total O.D. and total area of MDC as a percent of total nuclear O.D. and total nuclear area, respectively. (CDI) average distance of MDC from the center of the nucleus, as a percentage of nuclear radius. (NOC) the number of MDC clusters, (SI) symmetry index of MDC clusters and (QSI) the number of quadrants occupied by MDC.

Table 3

Means and standard deviations (SD) for the high density component (HDC) of 8C Malpighian tubule nuclei from high activity adult male, M. domestica.

Feature	1 day	8 day	14 day
	Mean ± SD	Mean ± SD	Mean ± SD
TOHDC	6.1 ± 7.0	9.7 ± 8.8	11.6 ± 7.4
TAHDC	2.8 ± 3.9	5.4 ± 5.5	5.9 ± 4.1
CDI	70.8 ± 17.6	49.6 ± 13.6	59.1 ± 14.3
NOC	2.7 ± 2.2	2.8 ± 1.6	3.4 ± 2.4
SI	0.2 ± 0.5	0.4 ± 0.6	0.3 ± 0.5
QSI	1.5 ± 0.7	1.4 ± 0.4	1.7 ± 0.9

Differences between the three age groups, for any feature, is not significant ($P > 0.05$). (TOHDC, TAHDC) total O.D. and total area of HDC as a percent of total nuclear O.D. and total nuclear area, respectively. (CDI) average distance of HDC from the center of the nucleus, as a percentage of nuclear radius. (NOC) the number of HDC clusters, (SI) symmetry index of HDC clusters and (QSI) the number of quadrants occupied by HDC.

Table 4

Means and standard deviations (SD) for the high density component (HDC) of 128C Malpighian tubule nuclei from high activity adult male, M. domestica.

Feature	1 day	4 day	8 day	14 day
	Mean ± SD	Mean ± SD	Mean ± SD	Mean ± SD
TOHDC	9.9 ± 8.8	10.8 ± 7.9	8.2 ± 6.6	18.5 ± 9.3*
TAHDC	5.3 ± 5.5	5.8 ± 4.9	4.1 ± 3.4	9.4 ± 5.3*
CDI	56.8 ± 11.5	53.3 ± 10.9	54.5 ± 5.0	51.5 ± 8.6
NOC	14.8 ± 7.8	14.0 ± 7.0	11.9 ± 6.4	17.9 ± 7.9
SI	0.5 ± 0.6	0.6 ± 0.6	0.4 ± 0.4	1.1 ± 0.6*
QSI	2.0 ± 0.7	2.1 ± 0.7	2.0 ± 0.5	2.6 ± 0.7*

The '*' indicates a significant difference ($P < 0.05$) when the feature is compared to that of the preceeding age group. (TOHDC, TAHDC) total O.D. and total area of HDC as a percent of total nuclear O.D. and total nuclear area, respectively. (CDI) average distance of HDC from the center of the nucleus, as a percentage of nuclear radius. (NOC) the number of HDC clusters, (SI) symmetry index of HDC clusters and (QSI) the number of quadrants occupied by HDC.

Table 5

Means and standard deviations (SD) for the medium density component (MDC) of 128C Malpighian tubule nuclei from high activity adult male, M. domestica.

Feature	1 day	4 day	8 day	14 day
	Mean ± SD	Mean ± SD	Mean ± SD	Mean ± SD
TOMDC	46.9 ± 12.7	53.8 ± 6.9*	52.4 ± 10.3	47.0 ± 7.9
TAHDC	34.7 ± 14.4	41.1 ± 8.5*	39.1 ± 10.1	35.6 ± 8.4
CDI	60.4 ± 4.3	59.2 ± 3.4	58.0 ± 1.9	58.2 ± 3.8
NOC	22.2 ± 16.8	12.4 ± 8.0*	14.6 ± 8.9	15.4 ± 10.5
SI	3.8 ± 1.6	4.5 ± 1.0	4.5 ± 1.5	4.1 ± 0.8
QSI	3.6 ± 0.5	3.7 ± 0.3	3.7 ± 0.4	3.7 ± 0.5

The '*' indicates a significant difference ($P < 0.05$) when the feature is compared to that of the preceeding age group. (TOMDC, TAMDC) total O.D. and total area of MDC as a percent of total nuclear O.D. and total nuclear area, respectively. (CDI) average distance of MDC from the center of the nucleus, as a percentage of nuclear radius. (NOC) the number of MDC clusters, (SI) symmetry index of MDC clusters and (QSI) the number of quadrants occupied by MDC.

Figure 10. Average Total nuclear DNA (expressed as Log_2 of total O.D.) as a function of age in high activity adult male, M. domestica.

□ 128C tubule

■ 64C tubule

◇ 8C tubule

⊕ Muscle

● Brain

All points represent the mean ± standard deviation.

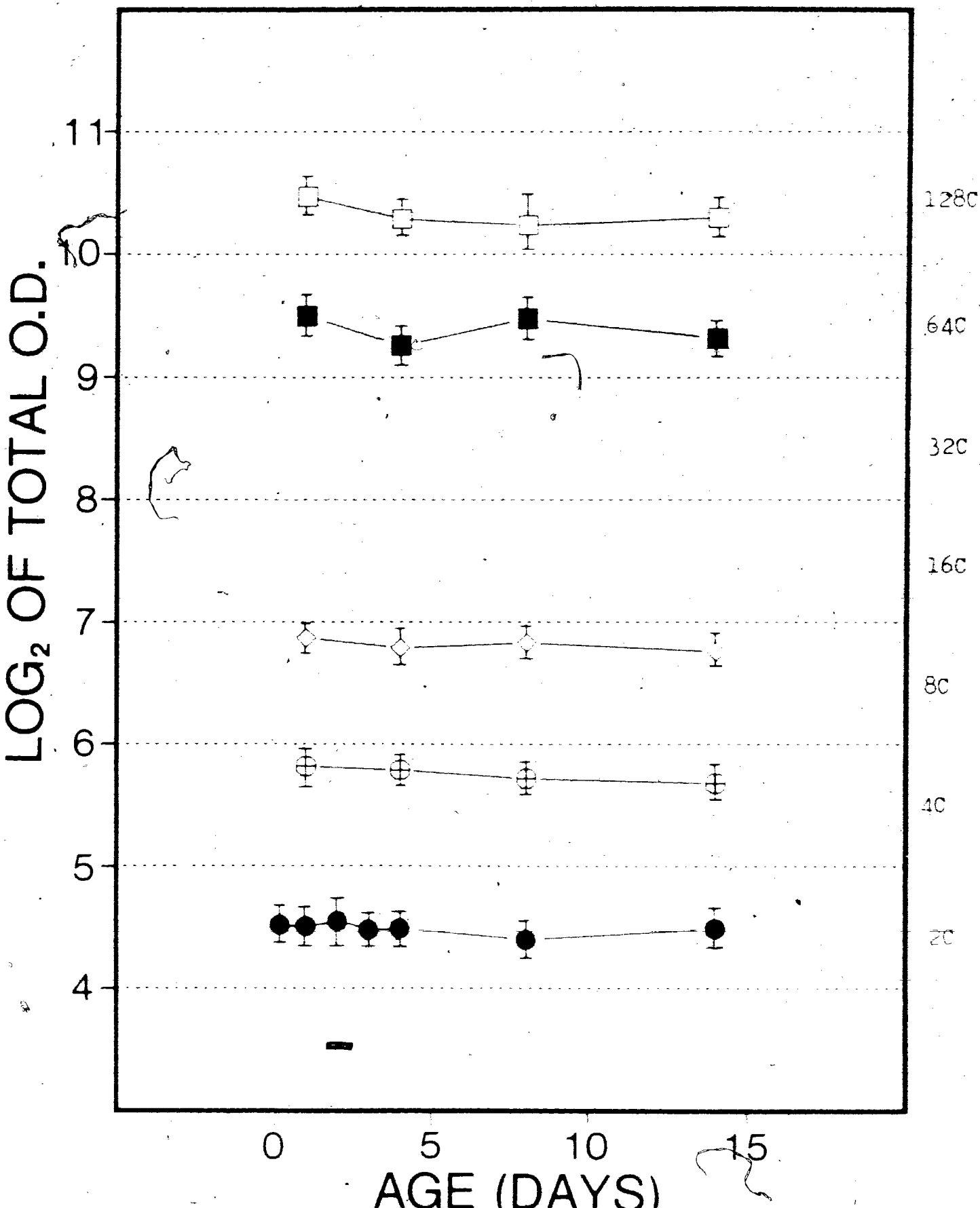
11
10
9
8
7
6
5
4
LOG2 OF TOTAL O.D.
0
5
10
15
AGE (DAYS)
128C
64C
32C
16C
8C
4C
2C

The dominant components in the tubule nuclei at day 1 (Fig. 11B) are LDC and MDC, each accounting for approximately 45% of total DNA. A significant reduction in LDC to 20% occurs by day 4 ($P < 0.01$). This reduction in LDC is accompanied by a significant increase in MDC to 60% and HDC to 18% ($P < 0.01$). The MDC fraction decreases significantly to 53% by day 8 ($P < 0.01$) while HDC increases to 29% ($P < 0.01$). The LDC does not change significantly between day 4 and day 8. The proportions of these three components remain unchanged between day 8 and day 14 ($P > 0.05$).

The dominant component in the muscle nuclei at day 1 is the LDC (Fig. 11C), which accounts for over 50% of total DNA, while MDC and HDC account for 32% and 11% respectively. The amount of HDC does not change significantly between day 1 and day 14 ($P > 0.05$). A slight but significant decrease in MDC occurs between day 1 and day 4 ($P < 0.05$), and is accompanied by an increase in LDC from 54% to nearly 60%. The amount of MDC increases significantly ($P < 0.01$) between day 4 and day 8 and again between day 8 and day 14, when it accounts for 40% of total DNA. This increase is associated with a proportional decrease in LDC to 40% of total DNA by day 14.

Subsequent results from the HA-group will be concerned with a closer examination of the HDC from the brain and tubule, and the MDC from the muscle. With two exceptions (described below), the magnitude of change in the MDC of the brain and tubule (Tables 6 and 7) is neglible compared to the HDC. HDC from the

Figure 11. Relative proportion of the low density, LDC (open bar), medium density, MDC (hatched bar) and high density, HDC (solid bar) components in brain (A), 64C tubule (B) and flight muscle (C) nuclei from high activity adult male, M. domestica. The amount of each component is expressed as a percentage of total DNA.

A: The relative proportions of LDC, MDC and HDC change significantly ($P < 0.01$) in brain nuclei between day 1 and day 4 with no significant change ($P > 0.05$) between day 4 and day 14.

B: The proportions of LDC, MDC and HDC change significantly ($P < 0.01$) in tubule nuclei between day 1 and day 8, with no significant change ($P > 0.05$) between day 8 and day 14.

C: The proportions of LDC, MDC and HDC change significantly ($P < 0.01$) in flight muscle nuclei throughout the 14 day interval.

The brain and tubule nuclei exhibit a progressive increase in the condensation state, whereas the condensation state of the muscle nuclei decreases before it increases.

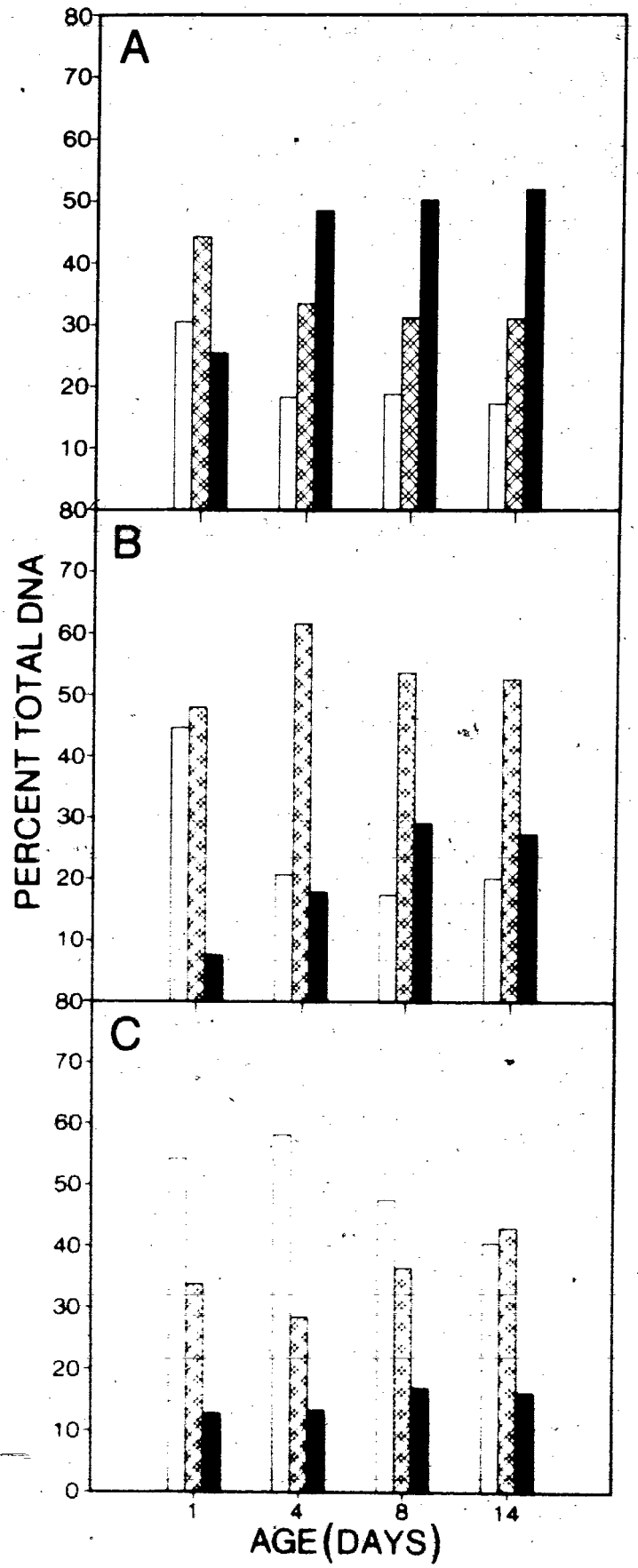
A
B
C
PERCENT TOTAL DNA
AGE (DAYS)
1
4
8
14
0
10
20
30
40
50
60
70
80

Table 6

Means and standard deviations (SD) for the medium density component (MDC) of brain nuclei from high activity adult male, M. domestica.

Feature	1 day	4 day	8 day	14 day
	Mean ± SD	Mean ± SD	Mean ± SD	Mean ± SD
TOMDC	44.2 ± 8.6	33.4 ±10.7*	31.1 ±10.7	31.0 ±10.4
TAMDC	29.4 ± 6.9	25.0 ± 6.4*	23.4 ± 6.8	23.9 ± 6.4
CDI	48.7 ± 5.3	58.0 ± 6.7*	58.5 ± 7.3	59.2 ± 6.9
NOC	1.7 ± 0.8	2.2 ± 1.0	2.3 ± 1.0	2.4 ± 1.1
SI	4.1 ± 1.4	3.4 ± 1.7*	3.3 ± 2.0	3.3 ± 2.1
QSI	3.2 ± 0.5	3.2 ± 0.5	3.1 ± 0.5	3.2 ± 0.5

The '*' indicates a significant difference ($P < 0.05$) when the feature is compared to that of the preceeding age group. (TOMDC, TAMDC) total O.D. and total area of MDC as a percent of total nuclear O.D. and total nuclear area, respectively. (CDI) average distance of MDC from the center of the nucleus, as a percentage of nuclear radius. (NOC) the number of MDC clusters, (SI) symmetry index of MDC clusters and (QSI) the number of quadrants occupied by MDC.

Table 7

Means and standard deviations (SD) for the medium density component (MDC) of 64C Malpighian tubule nuclei from high activity adult male, M. domestica.

Feature	1 day	4 day	8 day	14 day
	Mean ± SD	Mean ± SD	Mean ± SD	Mean ± SD
TOMDC	47.8 ±11.6	61.5 ±10.0*	53.5 ±13.8*	52.5 ±11.2
TAMDC	33.5 ±13.2	51.6 ± 8.2*	48.3 ±11.2	46.6 ± 9.6
CDI	62.7 ± 4.2	60.9 ± 3.8	64.3 ± 5.5	62.7 ± 5.4
NOC	27.4 ±15.4	5.1 ± 4.0*	6.5 ± 6.1	6.9 ± 5.7
SI	3.6 ± 1.4	5.7 ± 1.1*	5.2 ± 1.2	5.0 ± 1.2
QSI	3.6 ± 0.4	3.8 ± 0.2	3.8 ± 0.1	3.7 ± 0.2

The '*' indicates a significant difference ($P < 0.05$) when the feature is compared to that of the preceeding age group. (TOMDC, TAMDC) total O.D. and total area of MDC as a percent of total nuclear O.D. and total nuclear area, respectively. (CDI) average distance of MDC from the center of the nucleus, as a percentage of nuclear radius. (NOC) the number of MDC clusters, (SI) symmetry index of MDC clusters and (QSI) the number of quadrants occupied by MDC.

Table 8

Means and standard deviations (SD) for the high density component (HDC) of flight muscle nuclei from high activity adult male, *M. domestica*.

Feature	1 day	4 day	8 day	14 day
	Mean ± SD	Mean ± SD	Mean ± SD	Mean ± SD
TOHDC	12.9 ± 9.0	13.4 ± 6.1	17.1 ± 13.2	16.3 ± 9.9
TAHDC	5.5 ± 4.8	4.7 ± 2.8	7.8 ± 6.7	7.8 ± 6.0
CDI	74.5 ± 13.9	72.5 ± 19.9	67.6 ± 13.9	66.5 ± 22.9
NOC	3.5 ± 2.3	3.1 ± 1.8	2.9 ± 1.7	3.2 ± 1.8
SI	0.2 ± 0.5	0.1 ± 0.4	0.4 ± 0.7	0.7 ± 1.0
QSI	1.7 ± 0.6	1.5 ± 0.6	1.8 ± 0.7	1.8 ± 0.6

Differences between the four age groups, for all features, are not significant ($P > 0.05$). (TOHDC, TAHDC) total O.D. and total area of HDC as a percent of total nuclear O.D. and total nuclear area, respectively. (CDI) average distance of HDC from the center of the nucleus, as a percentage of nuclear radius. (NOC) the number of HDC clusters, (SI) symmetry index of HDC clusters, and (QSI) the number of quadrants occupied by HDC.

muscel nuclei did not change significantly with age (Table 8).

Fig. 12A shows the total O.D. of the HDC (TOHDC) with age in the brain and tubule nuclei. TOHDC increases significantly in the brain from 20.8% of total DNA in the 4-hour group to a maximum of 48.4% by day 4 ($P < 0.01$). TOHDC increases significantly in the tubule nuclei as well ($P < 0.01$), from 7.6% in the 1-day group to a maximum of 29.1% by day 8 (Fig. 12A).

The total area occupied by HDC (TAHDC), increases significantly ($P < 0.01$) in the brain from 7.9% in 4-hour-old flies to 22.2% by day 4 (Fig. 12B). TAHDC increases significantly ($P < 0.01$) in the tubules from 3.5% at day 1 to 18.7% by day 8 (Fig. 12B). TAHDC and TOHDC do not change significantly after day 4 in the brain, and after day 8 in the tubule ($P > 0.05$).

Total nuclear area (TNA) in the tubule and brain decreases significantly ($P < 0.01$) in parallel with the increase in the amount of HDC (Fig. 12C and 12D). The tubules, however, show an increase in the amount of HDC between day 4 and day 8 (Fig. 12A), while the total nuclear area remains constant over this time period. This may be due in part to the fact that both MDC and HDC increase between day 1 and day 4, but only the HDC increases between day 4 and day 8 (Fig. 11B).

Two dimensional symmetry analysis of the condensation event shows that the distribution of the HDC becomes more symmetrical with age in both the brain and tubule nuclei (Fig. 13A). The symmetry index (SI) for the 4-hour-old flies increases

Figure 12. HDC and global features for brain and 64C tubule nuclei from the high activity adult male, *M. domestica*.

All points represent the mean ± S.E.

A: Total O.D. of HDC (TOHDC)

B: Total Area of HDC (TAHDC)

C: Total nuclear area (TNA) of tubule nuclei

D: Total nuclear area (TNA) of brain nuclei.

● brain, ■ tubule.

Image features (A,B), global features (C,D).

Analysis summary: TOHDC and TAHDC increase significantly ($P < 0.01$) in the brain and tubule nuclei between day 1 and 4 and between day 1 and day 8, respectively. No significant change ($P > 0.05$) occurs between day 4 and 14 in the brain and between day 8 and 14 in the tubule. Brain and tubule TNA decreases significantly ($P < 0.01$) between day 1 and day 4, with no significant change ($P > 0.05$) between day 4 and day 14.

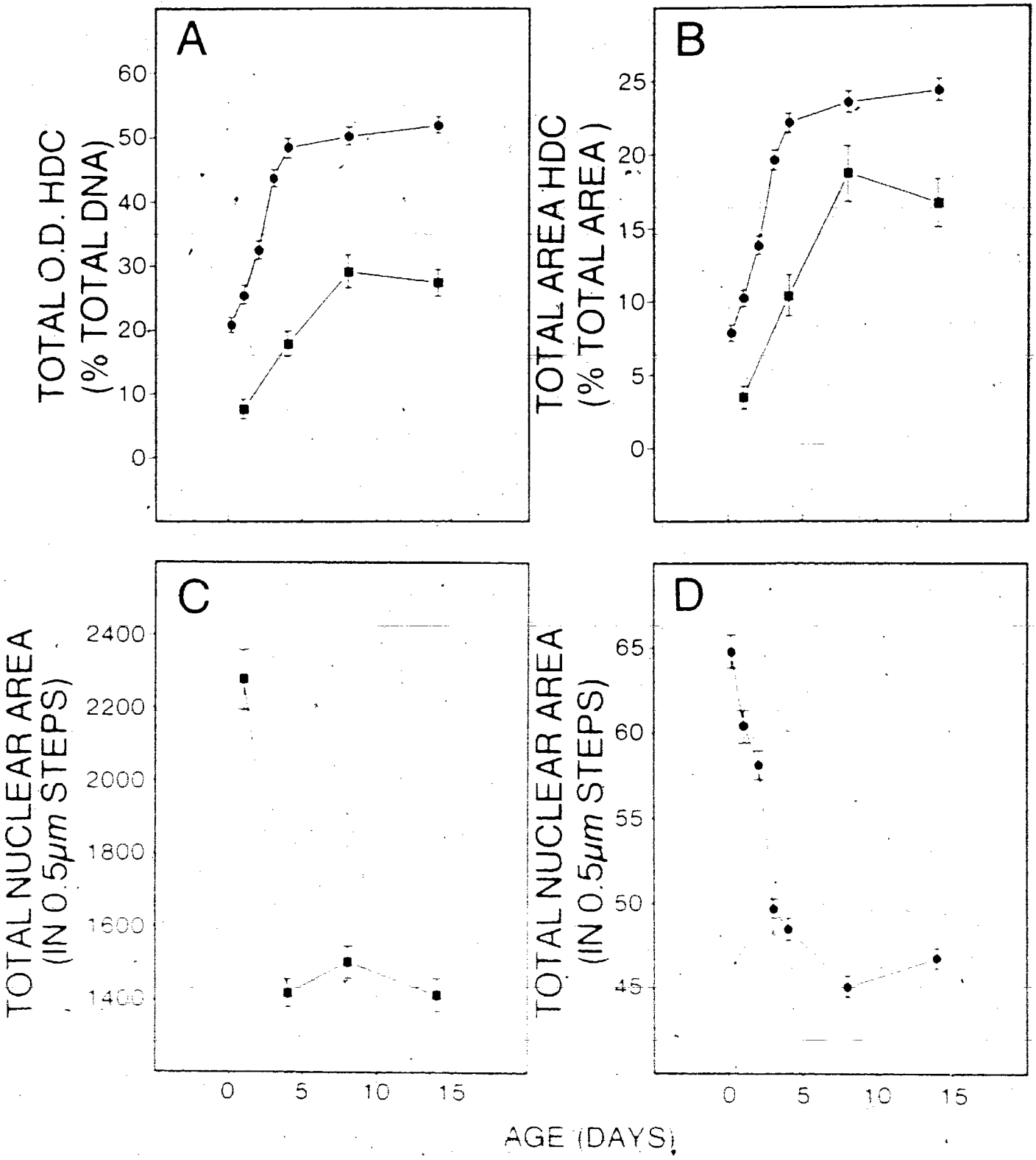
A
B
C
D
TOTAL O.D. HDC
(% TOTAL DNA)
TOTAL AREA HDC
(% TOTAL AREA)
TOTAL NUCLEAR AREA
(IN 0.5μm STEPS)
TOTAL NUCLEAR AREA
(IN 0.5μm STEPS)
AGE (DAYS)
0
5
10
15
0
10
20
30
40
50
60
0
5
10
15
20
25
1400
1600
1800
2000
2200
2400
45
50
55
60
65

significantly from a value of 0.48 (indicating an asymmetric distribution) to 4.6 by day 4 ($P < 0.01$). SI also increases significantly in the tubule from 0.27 at day 1 to a maximum of 2.26 by day 8 ($P < 0.01$).

The actual number of quadrants occupied by HDC (QSI) for each age group is shown in Fig. 13B. The HDC in the brain nuclei is restricted to essentially 1 quadrant in the 4-hour group, spreading to occupy 2.7 quadrants by day 4 ($P < 0.01$). The spread of the HDC in the tubule nuclei is in contrast to that of the brain, in that it occupies 1.8 quadrants at day 1 and does not attain a maximum of 2.6 quadrants until day 8 ($P < 0.01$). SI and QSI do not change significantly after day 4 in the brain, and after day 8 in the tubule ($P > 0.05$).

HDC appears as approximately 1 cluster in the brain nuclei and 12 clusters in the tubule nuclei. This does not change with age ($P > 0.05$). Moreover, the number of MDC clusters in the brain nuclei also remains constant with age (Table 6). However, MDC appears in the tubule nuclei as 27 distinct clusters in the 1-day group, but decreases significantly ($P < 0.01$) to 5 separate clusters by day 4, remaining constant up to day 14 (Fig. 13C). Fig. 13D shows the distance of the clusters from the geometric center of the nucleus (CDI). CDI of the medium and high density components in the tubule nuclei is usually about 60% of the nuclear radius and this does not change significantly with age. CDI for the MDC and HDC in the brain nuclei does show significant changes with age. The distance of the MDC clusters

Figure 13. Symmetry and cluster features in brain and 64C tubule nuclei from the high activity adult male, M. domestica.

All points represent the mean ± S.E.

A: The symmetry index of HDC (SI).

● brain, ■ tubule.

B: The number of quadrants occuppied by HDC (QSI).

● brain, ■ tubule.

C: The number of medium density clusters (MDC).

⊕ brain, ⊞ tubule.

D: MDC and HDC cluster distance index (CDI).

○ brain MDC, ● brain HDC.

Analysis summary: SI and QSI increase significantly ($P < 0.01$) in brain and tubule nuclei between day 1 and 4 and between day 1 and 8, respectively. No significant change ($P > 0.05$) occurs between day 4 and day 8. The number of MDC clusters decreases significantly ($P < 0.01$) in tubule nuclei between day 1 and day 4, with no change between day 4 and 8 ($P > 0.05$). The number of MDC clusters in brain nuclei does not change with age ($P > 0.05$). CDI (of brain MDC and HDC) shows significant change between day 1 and 4 ($P < 0.01$).

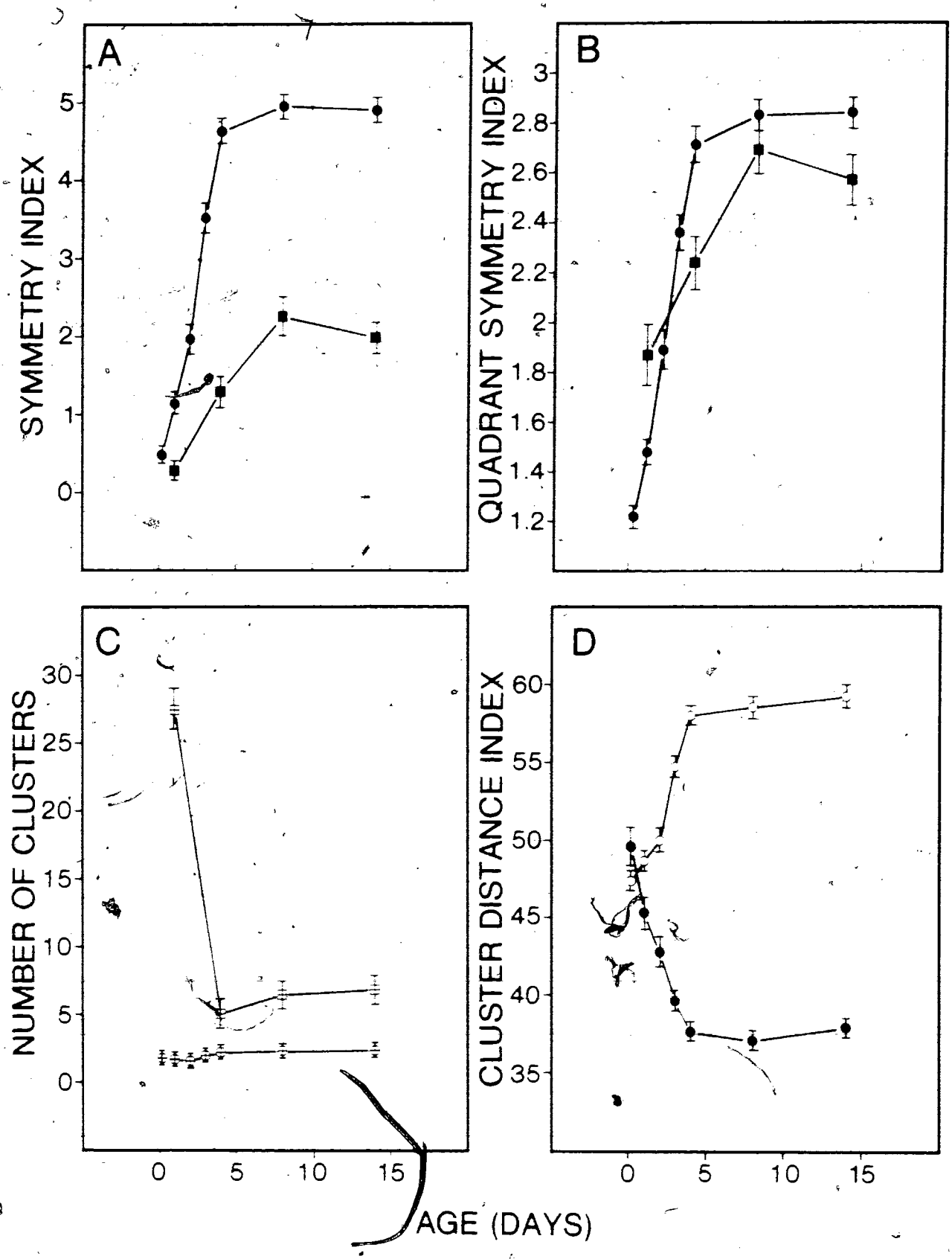
A
SYMMETRY INDEX
0
1
2
3
4
5
B
QUADRANT SYMMETRY INDEX
1.2
1.4
1.6
1.8
2
2.2
2.4
2.6
2.8
3
C
NUMBER OF CLUSTERS
0
5
10
15
20
25
30
D
CLUSTER DISTANCE INDEX
35
40
45
50
55
60
0
5
10
15
AGE (DAYS)

from the nuclear center is 47% of the nuclear radius in the 4-hour group and increases significantly to 58% by day 4 ($P < 0.01$). CDI of HDC is 50% in the 4-hour group, decreasing significantly to 38% by day 4 ($P < 0.01$). This represents a complementary shift where the HDC displaces the MDC toward the perimeter as it moves toward the center of the nucleus. Once this shift is complete, the brain nucleus contains a core of high density chromatin, with a surrounding shell of medium density, and possibly low density, chromatin.

Fig. 14A shows the total O.D. of the MDC in flight muscle nuclei. MDC in the flight muscle accounts for 41.9% of total DNA at day 1, but decreases significantly to 37.4% by day 4 ($P < 0.05$). A significant ($P < 0.01$) increase to 45.8% is observed between day 4 and day 8, and again between day 8 and day 14, at which time it accounts for nearly 43% of total DNA. TNA (Fig. 14B) does not change significantly between day 1 and day 4 ($P > 0.05$) but does decrease significantly between day 4 and day 8 ($P < 0.01$). The decrease in MDC between day 1 and day 4, with a parallel increase in LDC (Fig. 11C), indicates the occurence of a decondensation event during this period. Decondensation followed by recondensation is also evident in NOC (Fig. 14C) and SI (Fig. 14D). As the decondensation event procedes, NOC increases significantly ($P < 0.01$) from 8.6 at day 1 to 11.4 by day 4. This is accompanied by a significant decrease in SI from 1.8 at day 1 to 1.1 by day 4 ($P < 0.01$). MDC occupies approximately 3 quadrants at day 1 and has a CDI of about

Figure 14. Image and global features for flight muscle nuclei from the high activity male, M. domestica.

The image features (A,C,D) were extracted from the medium density component (MDC).

All points represent the mean ± S.E.

A: Total O.D. of MDC (TOMDC).

B: Total nuclear area (TNA).

C: The number of MDC clusters (NOC)

D: MDC symmetry index (SI).

Analysis summary:

TOMDC and SI decrease significantly ($P < 0.05$) between day 1 and 4 followed by a significant ($P < 0.01$) increase between day 4 and day 14. TNA decreases significantly ($P < 0.01$) between day 4 and 8, with no significant change ($P > 0.05$) between day 1 and day 4 or between day 8 and 14. NOC increases significantly ($P < 0.01$) between day 1 and 4 and decreases significantly between day 1 and day 8 ($P < 0.01$), with no significant change after day 8 ($P > 0.05$).

TOTAL O.D. MDC
(% TOTAL DNA)
25
30
35
30
45
50
A
NUMBER OF CLUSTERS
4
6
8
10
12
14
C
0
5
10
15
AGE (DAYS)
TOTAL NUCLEAR AREA
IN 0.5um STEPS
120
170
220
270
320
375
B
SYMMETRY INDEX
1
2
3
D

67%. Neither of these features change with age ($P > 0.05$).

Fig. 15A shows the LDC, MDC and HDC in the brain from the low activity group. The proportions at day 1 in the brain of the LA-group are similar to the 1-day brain of the HA-group. A significant shift occurs in the brain of the LA-group between day 1 and day 4 as it does in the brain of the HA-group (Fig. 15B), but the amounts of HDC at day 4 and day 14 are significantly ($P < 0.01$) less than those in the HA-group, indicating a lower condensation state in the brain nuclei of the LA-group during this period. The day 4 proportions in the brain of the LA-group remain unchanged through to day 14 ($P > 0.05$).

Table 9 shows the values for additional image features in the 1-day to 14-day HA and LA groups. There are few significant differences between the HA and LA groups at day 1 but several significant differences occur by day 4 and day 14. Total nuclear area is significantly greater in the LA-group at day 4, but is not significantly different from the HA-group at day 14. At day 4 and day 14, the brain nuclei of the LA-group have significantly less HDC which displays an asymmetric distribution pattern characteristic of a day 1 nucleus from either the LA or HA group.

Tables 10 and 11 show the training sets for the high activity brain and tubule, respectively. The Merit values for each feature used are also shown. These values range from 0 to 1. Generally, discrimination is high when the feature has a

Figure 15. The relative proportions of the low density, LDC (open bar), medium density, MDC (hatched bar) and high density, HDC (solid bar) components in brain nuclei from the adult male, M. domestica.

A: Low activity (LA) group.

B: High activity (HA) group.

Analysis summary: The relative proportions of LDC, MDC and HDC change significantly ($P < 0.01$) between day 1 and 4 in both the LA and HA groups, with no significant change ($P > 0.05$) between day 4 and day 14. Comparisons between the HA and LA groups show that the amount of the three components is not significantly different at day 1 ($P > 0.05$) but that the day 4 and day 14 proportions of MDC and HDC are significantly different ($P < 0.01$). The brain nuclei of the LA-group have relatively less HDC by day 4 and 14, as compared to the HA-group, and is therefore in a lower condensation state.

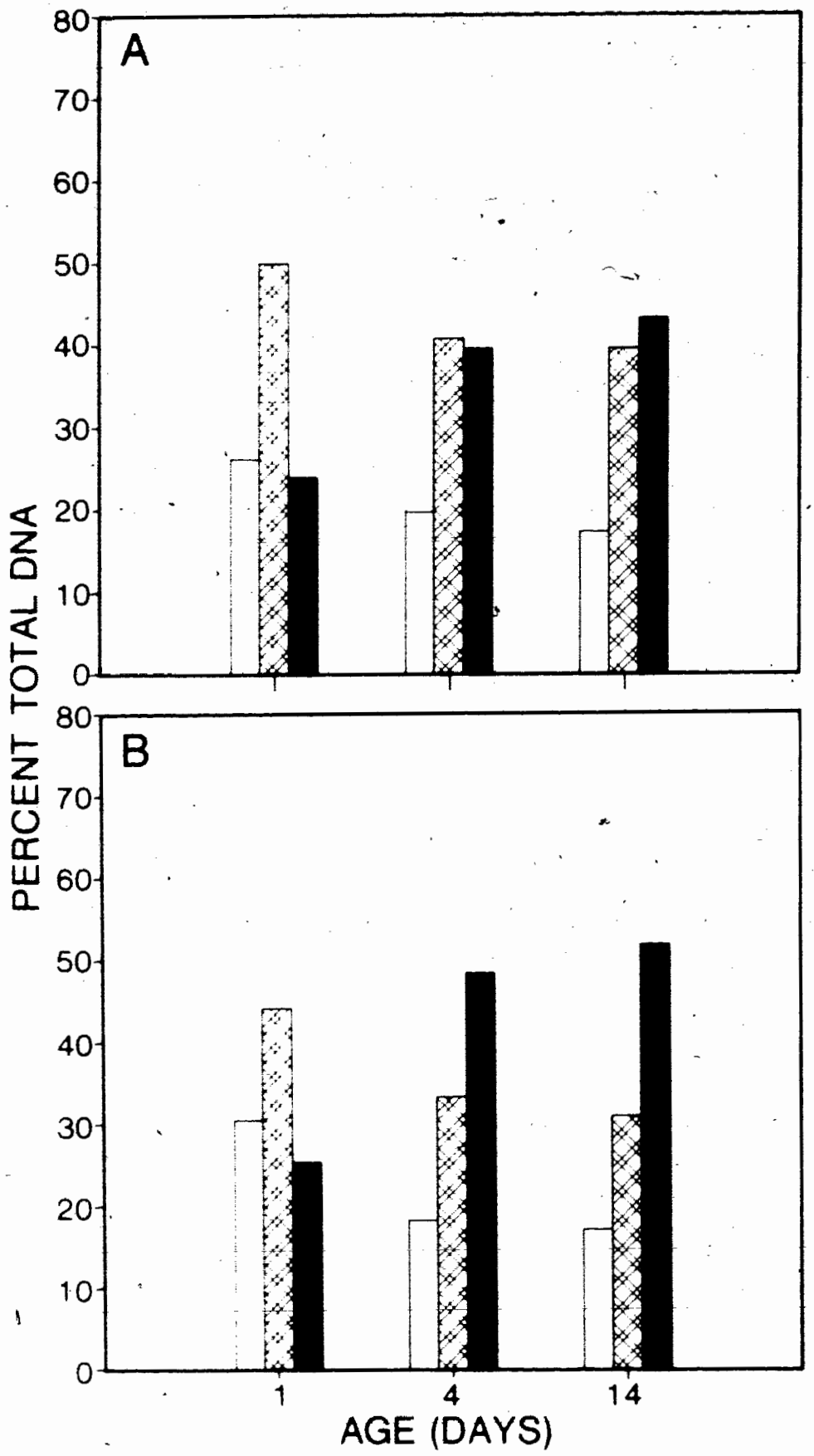
A
B
80
70
60
50
40
30
20
10
0
PERCENT TOTAL DNA
1
4
14
AGE (DAYS)

Table 9

A comparison of brain nuclei of adult male, M. domestica from high (HA) and low (LA) activity groups.

Feature	1 day		4 day		14 day	
	LA	HA	LA	HA	LA	HA
TNA	57.4	59.0	50.6	47.9**	44.9	46.5
TAHDC	8.9	10.3*	15.9	22.2**	18.9	24.3**
CDI	48.9	45.3	41.0	37.7	36.0	38.0*
NOC	1.2	1.1	1.1	1.1	1.0	1.1
SI	0.5	1.0*	2.7	4.6**	4.1	4.9*
QSI	1.3	1.5	2.0	2.7**	2.5	2.8**

* ($P < 0.05$) ** ($P < 0.01$)

(TNA) total nuclear area, (TAHDC) total area of HDC as a percent of total nuclear area, (CDI) average distance of MDC from the center of the nucleus, expressed as a percent of nuclear radius, (NOC) the number of MDC clusters, (SI) symmetry index of MDC clusters and (QSI) the number of quadrants occupied by MDC.

Table 10

Training set for the 1-day and 14-day-old brain nuclei from the high activity adult male, M. domestica.

Image Feature	Merit	Decision Boundary	Decision Rule
Total nuclear area	0.529	61.50	A
Total O.D of HDC	0.692	47.34	B
Total area of HDC	0.721	24.74	B
Cluster distance	0.279	53.76	A
Symmetry index	0.643	1.53	B
Quadrant symmetry	0.620	1.14	B

The merit value will range from 0 to 1 and represents an estimate of how well the feature discriminates between the two groups. Generally, discrimination is high when the features have merit values greater than 0.5.

Decision rules:

A If the feature value is greater than the decision boundary assign the nucleus to the 1-day-old group.

B If the feature value is greater than the decision boundary assign the nucleus to the 14-day-old group.

Table 11

Training set for the 1-day and 14-day-old 64C Malpighian tubule nuclei from the high activity adult male, M. domestica.

Image Feature	Merit	Decision Boundary	Decision Rule
Total nuclear area	0.717	2191	A
Total area of HDC	0.462	5.06	B
Quadrant symmetry	0.338	2.93	B

The merit value will range from 0 to 1 and represents an estimate of how well the feature discriminates between the two groups. Generally, discrimination is high when the features have merit values greater than 0.5.

Decision rules:

A If the feature value is greater than the decision boundary assign the nucleus to the 1-day-old group.

B If the feature value is greater than the decision boundary assign the nucleus to the 14-day-old group.

merit value greater than 0.5. Classifications based on these training sets, are shown in Table 12. Classification of the muscle was not done due to the biphasic nature of the condensation event. The classifications show that the changes in the brain nuclei have stabilized and produced a homogeneous population by the fourth day. 82% of the 8-day group and 86% of the 4-day group were classified with the 14-day group, while 94% of the 4-hour group was classified with the 1-day group. Classification of the 2-day group shows that only 67% can be classified with the 1-day group, reflecting the fact that these nuclei are in a state of change throughout this period.

Classification of the tubule nuclei shows that 84.4% of the 4-day nuclei were classified with the 14-day group, while 62.5% of the 8-day nuclei were classified with the 14-day nuclei. Classification of the brain from the LA-group, using the HA-group training set from Table 10, shows that 64% of the 4-day LA-group and 60% of the 14-day LA-group are classified with the 1-day HA-group, in contrast to the classification of the 4-day HA-group where only 14% are classified with the 1-day HA-group.

Computerized images of 64C tubule nuclei from the 1-day and 14-day group are shown in Fig. 16. These nuclei were selected by a program which evaluates all nuclei in each group with respect to how well they represent the group mean in all features considered. The general trends involving total nuclear area, MDC and HDC are clearly evident.

Table 12

Classification of brain and 64C tubule nuclei from high and low activity (HA, LA) adult male, M. domestica.

Group	Age	Classification	
		1-day	14-day
HA-brain	4-hour	94.0%	6.0%
HA-brain	1-day	83.0%	17.0%
HA-brain	2-day	67.0%	33.0%
HA-brain	3-day	34.0%	66.0%
HA-brain	4-day	14.0%	86.0%
HA-brain	8-day	18.0%	82.0%
HA-brain	14-day	5.0%	95.0%
HA-tubule	1-day	100.0%	0.0%
HA-tubule	4-day	15.6%	84.4%
HA-tubule	8-day	37.5%	62.5%
HA-tubule	14-day	19.0%	81.0%
LA-Brain	1-day	96.0%	4.0%
LA-Brain	4-day	64.0%	36.0%
LA-Brain	14-day	60.0%	40.0%

Classification of the brain (HA and LA) and tubule is based training sets in Tables 10 and 11, respectively.

Figure 16. Computerized images of 64C tubule nuclei from high activity adult male, M. domestica, which are representative of the 1-day (A) and 14-day (B) groups. These images were selected by a program that evaluates all nuclei in each age group with respect to how well they represent the group mean in all features considered. These images show the significant decrease in total nuclear area, the increase in the amount of HDC, the change in the HDC spatial distribution and the decrease in the number of MDC clusters. □ LDC, ⊞ MDC, ■ HDC.

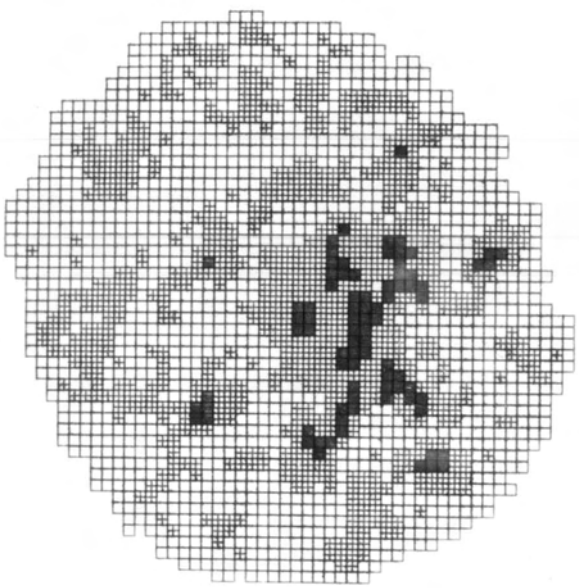

A

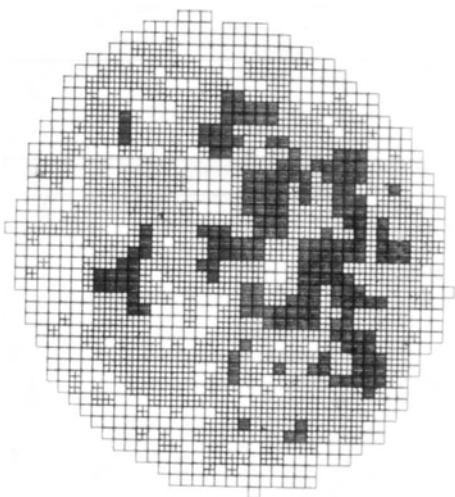

B

DISCUSSION

Age-related studies of cell nuclei have frequently been concerned with total DNA content or the structural and functional properties of chromatin. The various studies concerned with total DNA content of a given cell type have failed to show a significant change with age in human brain (Lapham, 1968) or in rat brain, kidney (Enesco, 1967), and liver (Bedi and Goldstein, 1978).

In the present study three different tissues were examined, representing five ploidy classes. No evidence could be found for a significant change in DNA content in any of these tissues. This is so despite the fact that nuclei from the muscle and tubules showed a 10-12% reduction in total optical density with age. This reduction is believed to be the result of decreased acid lability of the DNA, as a consequence of the condensation event (Brachet et al., 1968; Badr, 1972). This would have the effect of reducing the amount of apurinic acid formed during the hydrolysis step of the Feulgen reaction, thereby lowering the total O.D. of the nucleus without an actual loss of DNA.

There was also no evidence for an age-related shift in ploidy class frequencies within the tubules, despite an apparent reduction in the 128C class in the 8-day and 14-day-old groups. This apparent shift was probably due to the fact that the male population is heterogeneous with respect to the ratio of 64C:128C tubule nuclei (Table 1).

Despite the lack of any evidence for an age-related change in DNA content, several studies have demonstrated an age-related increase in the thermal stability of chromatin (von Hahn, 1970), and increased resistance to salt dissociation, coupled with reduced transcriptional activity (O'Meara and Herrmann, 1972), suggesting a condensation event with a subsequent reduction in the activity of the nucleus. The results of pattern analysis have also indicated an age-related increase in the condensation state of nuclei from brain, Malpighian tubule and flight muscle of the adult male, M. domestica.

The general relationship between the degree of chromatin condensation and its transcriptional activity has been examined in interphase nuclei at the microscopic (Harris, 1967; Panar and Nair, 1975), ultrastructural (Frenster et al., 1963; Littau et al., 1964; Lamb and Daneholt, 1979; Hamkalo and Rattner, 1980) and molecular levels (Weintraub and Groudine, 1979; see review by Weisbrod, 1982). This relationship has also been studied in polytene chromosome puffs (Ashburner, 1972; Daneholt, 1975), lambrush chromosomes (Rogers and Browder, 1977) and in spermatid nuclei during spermiogenesis (Monesi, 1965; see discussion by Browder, 1980). All of these studies have shown an inverse relationship between chromatin condensation and transcriptional activity, implying that the activity level of the nucleus and the cell as a whole can be monitored by analyzing the interphase condensation pattern.

In this regard, pattern analysis is fundamentally concerned with the visible effects (at the microscopic level) that a condensation event might have on the interphase nucleus. Micrographs of cell nuclei from various mammalian tissues show that the condensed chromatin frequently appears near, and in many cases actually lines, the nuclear envelope (Porter and Bonneville, 1973) Studies of interphase nuclei suggest that chromatin is organized into 38 to 80 kilo bp supercoiled complexes of DNA (Igo-Kemenes and Zachau, 1978; Vogelstein et al., 1980) that appear to be anchored directly to the nuclear envelope (Hancock and Hughes, 1982). This is thought to explain the fact that condensation of chromosomes, during early prophase, occurs near the nuclear membrane (Comings and Okada, 1971; McKeon et al., 1984). It could also explain the fact that the heterochromatinized X chromosome (Barr body) of mammalian females, occurs near the nuclear membrane (Brown, 1966; Lyon, 1974), and the peripheral location of condensed chromatin in interphase nuclei. Thus a condensation event in an interphase nucleus should be accompanied by a significant redistribution of the chromatin, characterized by a peripheral shift and spatial redistribution of the condensed component.

In the present study, an application of pattern analysis showed that the condensation state of brain, tubule and flight muscle nuclei increases with age and that the time course of the event and the spatial distribution of high and medium density components is tissue specific. In addition, the muscle nuclei

showed a unique decondensation event prior to an increase in its condensation state.

These results were obtained by using six image features, in addition to two global features relating to the total O.D. and total area of the nucleus. Two of the image features, Total O.D. and total area of the medium (TOMDC TAMDC) and high density components (TOHDC,TAHDC), simply estimate the magnitude of the condensation event, while The feature NOC estimates the number of these clusters. The cluster distance index (CDI) is intended to detect a peripheral shift of the clusters, if it occurs, while the symmetry features estimate the degree to which the two dimensional spatial distribution of a given component has changed, given a condensation event.

My results indicated a peripheral shift in a medium density component (MDC) in brain nuclei and was associated with an unusual central shift of a high density component (HDC). I did not find evidence for a peripheral or central shift in either the MDC or HDC of the tubule and muscle nuclei. However, nuclei from all of these tissues showed significant alterations in the distribution pattern, as defined by symmetry analysis, in MDC and HDC. The brain and tubule nuclei showed the most significant change in the HDC with the MDC remaining relatively stable. The two major exceptions to this involved the peripheral shift of MDC in the brain nuclei and the reduction in the number of MDC clusters in the tubule nuclei.

The symmetry features can also estimate the extent to which the chromosome population is involved in the condensation event. This estimate is based on the assumption that each chromosome is restricted to a specific domain of approximately equal area. The justification for this assumption is based on the fact that the condensation of chromosomes during early prophase occurs in a symmetrical distribution around the nuclear envelope. (Comings and Okada, 1971; McKeon et al., 1984). Symmetry analysis (appendix I) assumes that the various chromosomes are distributed evenly over a four quadrant, two dimensional coordinate system. If this assumption is correct, a condensation event involving all chromosomes (or parts of all chromosomes) would result in a significant increase in the distributional symmetry (ie. the symmetry index, SI) of the component in question. On the other hand, if the condensation event involved only a fraction of all chromosomes then the symmetry index would change very little, if at all.

In addition, estimating the number of quadrants occupied by the condensed component (the quadrant symmetry index, QSI) is equivalent to estimating the fraction of the nuclear image that is involved in the condensation event. For example, a QSI of 1.0 represents 1.0/4.0, or 25% of the nuclear image. My results show that 75% of the brain nuclear image, from the high activity group, is affected by the increase in the high density component (HDC), whereas the total area of HDC is only 24% of total

nuclear area by day 14. Since 24% of the total nuclear area will fit within one quadrant, the total area of HDC alone does not give an accurate estimate of how global the condensation event is. Similarly, the HDC condensation event in the tubule nuclei affects 65% of the nuclear image, while the total area of HDC is only 17% of total nuclear area. Finally, the MDC condensation event in the muscle nuclei affects 75% of the nuclear image while the total area of MDC at day 14 is only 30% of total nuclear area. The significant increase in the symmetry index (SI) and the difference between QSI and the total areas of MDC and HDC indicate that the condensation event in all of these nuclei is affecting most, if not all, of the chromosomes.

Further characterization of the condensation event in brain and tubule nuclei was obtained by a classification procedure, referred to as discriminant analysis. Classification of the brain nuclei, from the high activity group, showed an age-dependent decrease in the number of nuclei classified with a 1-day-old model, coupled with an increase in the number of nuclei classified with a 14-day-old model. The 1-day and 14-day models constitute the training set, to which all the other age groups are compared. Classification of the tubule nuclei did not show as clear a trend as did the brain. This was largely due to the fact that a condensation event occurred in the tubule between day 1 and 4 and again between day 4 and 8. This means that the 4-day group had both 1-day and 14-day character. The fact that the majority of the 4-day group was classified with

the 14-day group does not mean that the two are identical, and indeed we know that they are not, but only that the 4-day group is more like the 14-day group than the 1-day group.

In this regard, it was possible to show that the brain nuclei from the 4-day-old low activity group have a lot of 1-day-old character. That is, the majority of the 4-day-old brain nuclei, from the high activity group, are classified with the 14-day-old high activity group, whereas the majority of the 4-day-old brain nuclei, from the low activity group, are classified with the 1-day-old brain nuclei. This suggests (along with the pattern analysis) that the final amount of HDC in the brain nuclei is related to the rate at which the male ages, as the low activity group had a mean lifespan nearly triple that of the high activity group.

The condensation event in the brain nuclei from the high activity group occurs during the peak activity period of the male, which extends from a few hours after emergence up until the third or fourth day (Clark and Rockstein, 1964). This condensation event precedes a significant decline in wing beat freguency and duration of flight by day 5 (Rockstein and Bhatnagar, 1966) and a loss of one or both wings in half the male population by day 6 (Fig. 6). Wing abrasion and loss may be due to a progressive decline in the circulation of hemolymph throughout the wing (Wigglesworth, 1970).

The male is believed to be mature by day 1, as mating begins 16 to 24 hours after emergence (Murvosh et al., 1964),

Ca-activated ATPase, brain cholinesterase (Clark and Rockstein, 1964) and thoracic acid phosphatase activities (Rockstein and Brandt, 1963) are all maximal within 24 hours of emergence. Moreover, it is pertinent to add that the female begins laying eggs on the fourth to the fifth day and she only mates once or twice throughout her life time. In addition, in all colonies examined, essentially all of the females have mated by day four (Adams and Hintz, 1969). These observations suggest that the role of the male is essentially complete by day 4. Hence, the condensation event in the brain appears to mark the end of the peak activity period of the male and the onset of outwardly apparent physical degeneration.

Other studies concerning age-related changes in the flight muscle of the male have shown the occurrence of early and late events. The early events include a significant decrease in thoracic levels of trehalose (Rockstein and Srivastava, 1967) and the activity of acid phosphatase (Rockstein and Brandt, 1963) during the first few days after adult emergence. These events, like the condensation event in the brain, precede the reduction in flight ability, loss of wings and decreased activity level cited above. The late events, including a decrease in the thoracic activity of NAD-dependent alpha glycerophosphate dehydrogenase (Rockstein and Brandt, 1963) and the thoracic levels of thiamine (Rockstein and Hawkins, 1970) begin after day 4 and could occur as a consequence of prior senescent events.

Pattern anlysis of the flight muscle nuclei showed an initial decondensation event between day 1 and 4. My data does not cover the second and third day, however, considering the fact that peak flight activity is attained between day 1 and 2 (Rockstein and Bhatnagar, 1966) it would seem likely that the decondensation event actually occurs during this period. Following the decondensation event the muscle nuclei appear to recondense between day 4 and day 14. It is during this period when significant wing loss, reduction in flight ability and the late biochemical events in flight muscle occur.

The condensation event in the Malpighian tubule occurred during both the early and late events and begins soon after emergence, as it does in the brain. Whether the condensation event in the brain is influencing the event in the tubules is difficult to say. From the data that I have collected it is only possible to conclude that the 64C tubule cells, and the flight muscle, appear to age more slowly than the brain cells.

The results of pattern analysis correspond with the maturation and senescence profile of the adult male, and are in general agreement with Clark and Rockstein (1964) and Rockstein and Bhatnagar (1966) that the male matures early (by day 1) and ages rapidly. In each tissue type that I examined there appears to be an inverse relationship between the condensation state of the nuclei and the activity level of the organism, implying that the activity level of the brain, tubule and muscle is maximal shortly after emergence, but decreases significantly during the

first four days. This is in contrast to the maturation and senescence profile of Drosophila (Miquel, 1971), the mosquito (Mills and Lang, 1976) and the blowfly (Levenbook and Williams, 1959) which are believed to have a more extended maturation period, lasting for 7 to 10 days after adult emergence.

The differences between the brain, tubule and flight muscle, with respect to the results of pattern analysis, may be relevant to certain gerontological theories such as the hypothalamic elevation theory of Dilman and Anisimov (1979) or the hypothalamic disregulation theory (see review by Everitt, 1980). These theories are primarily concerned with the control of the pituitary gland by the hypothalamus.

A major consequence of the hypothalamic theories is that an age-related change in specific brain cells could serve to regulate the rate at which the whole organism ages. Moreover, these theories suggest that an organism may represent a mosaic with respect to the rate at which various cell and tissue types age. Organ transplant studies (Peng and Huang, 1972; Pecile et al., 1966) and regional differences in the age-related decline in human brain neurotransmitters and related enzymes (McGeer and McGeer, 1981), indicate that such a mosaic exists. The results of pattern analysis also indicates the existence of a mosaic, in this case involving brain, tubule and flight muscle nuclei. This mosaic pertains to the time course of the condensation event and to the condensation pattern, which appears to be both tissue and age specific.

The significant changes that were shown to occur in the nuclei of the brain and Malpighian tubules may reflect progressive deterioration of the visual system, followed by the excretory system. Failure of the latter system could be a major cause of mortality in laboratory-reared flies. However, practically nothing is known about age-related biochemical changes in either the optic lobes or the Malpighian tubules.

The magnitude of the condensation event in the brain is reminiscent of the chromatin condensation that occurs during spermiogenesis (Browder, 1980; Perreault et al. 1984) and the possiblity exists that the former event could involve some degree of histone substitution or nucleosome polymerization through an increase in disulfide bonds. An age-related increase in the disulfide:sulfhydryl ratio has been demonstrated in whole body chromatin of the blowfly (Tas, 1978).

The condensation event in the brain could also be inititated by an age-specific phosphorylation of the nucleosome histone H1 or a specific H1 subtype (Renz et al., 1977; Kozo, et al., 1981). The condensation event in the Malpighian tubules and flight muscle nuclei could also involve some or all of these processes. The possiblity exists that the condensation event could affect the activity level of these cells, either through the inverse relationship between the condensation state of the nucleus and its transcriptional activity, or through an interference with the hormonal control of gene expression, as suggested by the results of Spelsberg et al. (1977) and Weisbrod

et al. (1980). However, the condensation event in itself is probably not the direct cause of reduced cellular activity but simply reflects a prior event (or set of events), at the level of the nucleosome, the exact nature of which is yet to be determined.

CONCLUSIONS

Computer analysis of digitized images of Feulgen-stained optic lobe , Malpighian tubule and flight muscle nuclei from the adult male housefly, M. domestica. has shown the following:

1. No age related change in total DNA content or ploidy class frequencies could be found in brain, muscle or Malpighian tubule nuclei.
2. The condensation state of brain and tubule nuclei tends to increase with age, although the time course of condensation event, and the distribution and relative proportions of the MDC and HDC are tissue specific. The most rapid change occurred in the brain followed by the tubule and muscle.
3. The condensation state of flight muscle nuclei decreases before it increases, indicating an initial decondensation event, which parallels the period of peak flight activity and flight muscle developement.
4. The condensation state of the type II neuron nucleus appears to be related to the rate at which the male ages since it was consistently lower in the low activity group than it was in the high activity group.
5. The lowest condensation state of a nucleus is associated with the highest activity level of the cell.
6. Pattern analysis supports hypothalamic theories of the aging process, as the brain, tubule and flight muscle do not appear to age uniformly.

APPENDIX I

Several programs were written during the course of this work. Two of these will be descibed here which deal with the analysis of the 2-dimensional symmetry of the interphase nucleus and with an automated procedure for processing and cleaning digitized nuclear images.

I). Analysis of Spatial Symmetry (SPATS)

This program extracts 3 symmetry features and one global anatomical feature which gives an estimate of the cross-sectional profile of the entire nucleus. These four features include:

1. Symmetry Index (SI)
2. Quadrant Symmetry Index (QSI)
3. Ring Symmetry Index (RSI)
4. Core Ratio (CORAT)

a. SYMMETRY INDEX

The symmetry index provides a measure of how evenly a particular component is distributed over the nuclear image. It accomplishes this by dividing the image into 4 quadrants, calculating the origin of the image (in array coordinates) and then converting the array location of each cluster into a set of (x,y) coordinates. This conversion is depicted in Fig. 17A. The array coordinates for row and column are shown along the left and bottom. As indicated, the array coordinate for the column and row will become the x and y coordinate

,respectively, in the (x,y) coordinate system. The row value increases from top to bottom and the columns increase from left ro right. The origin of the image has the array coordinates (9,11) which corresponds to the position (0,0) in an (x,y) coordinate system. From this diagram we can derive two simple expressions which allow us to convert any array location to an (x,y) coordinate system:

x = column - column origin

y = row origin - row

By using these expressions we can then take advantage of the properties of symmetry coordinates. For any point (x,y) we can easily find 3 points which are distributed over the remaining 3 quadrants in a perfectly symmetrical pattern relative to the original point. These points are (-x,y), (-x,-y) and (x,-y). Each of these points represent a symmetry coordinate of the original point. The location of these points is shown in Fig. 17B. If we let 'n' be the number of points in a component of interest, and if each point can have 3 symmetry coordinates, then the total number of symmetry coordinates possible is 3n. By determining the actual number of symmetry coordinates 'b' that an image has enables us to calculate SI:

$$SI = b/3n + 4a$$

The factor 4a is included to allow for the case where a given component has a point at the origin (0,0) of the image. That is, The point (0,0) is defined as having 4 symmetry coordinates. If this occurs a = 1, otherwise a = 0 and the factor drops out of the equation. This ratio is multiplied by 10 to force SI to take on values between 0 and 10. The image in Fig. 17B has a symmetry index of 10.0, whereas SI is 0 for the image in Fig. 17C.

If we consider Fig. 18C more closely we can see that SI would be greater than zero if the cluster were to lie on one of the axes. Such a situation could easily occur since the orientation of a nuclear image in an array is purely random. SPATS allows for a random orientation by rotating the axis and analyzing the image four times at an axial rotation of 0,20,45, and 70 degrees. SI is calculated for each rotation and the minimum is taken as the best estimate. At axial rotations of 0 and 45 degrees the symmetry coordinates are obtained by taking the appropriate negative and negative inverse of the original coordinate. At axial rotations of 20 and 70 degrees the symmetry coordinates must be obtained trigonometrically.

b. QUADRANT SYMMETRY INDEX (QSI)

QSI provides an estimate of the number of quadrants occupied by a component of interest. As with SI, determining QSI is complicated by the problem of random orientation and is dealt with in the same manner by estimating QSI at four axial rotations. The angular rotations are the same as for SI. At an angular rotation of 0 degrees a point can be assigned to any of the four quadrants simply by converting their array location to an (x,y) coordinate. However when the axis is rotated some angle θ each point must be tested using 4 rules to see if the point falls within a test area. The test areas are shown in Fig. 17D. The 4 rules are listed below:

1) (When $x > 0$ and $y > 0$)

   If $y > x(\text{TAN } \theta)$ assign the point to quadrant 1, otherwise assign it to quadrant 4.

2) (When $x < 0$ and $y > 0$)

   If $x > y(\text{TAN } \theta)$ assign the point to quadrant 2, otherwise assign it to quadrant 1.

3) (When $x < 0$ and $y < 0$)

   If $y > x(\text{TAN } \theta)$ assign the point to quadrant 3, otherwise assign it to quadrant 2.

4) (When $x > 0$ and $y < 0$)

   If $x > y(\text{TAN } \theta)$ assign the point to quadrant 4,

Figure 17. Algorithm for symmetry analysis.

A: Position of a nuclear image in a 2 dimensional array indicating the conversion of (row,column) coordinants to (x,y) coordinants. The row increases from top to bottom, columns increase from left to right

B: Location of three symmetry coordinants for the point (x,y),

C: Location of 4 points when the symmetry index equals zero.

D: The location of the test areas (hatched region) used to assign a point to a particular quadrant after the axis has been rotated by some angle θ

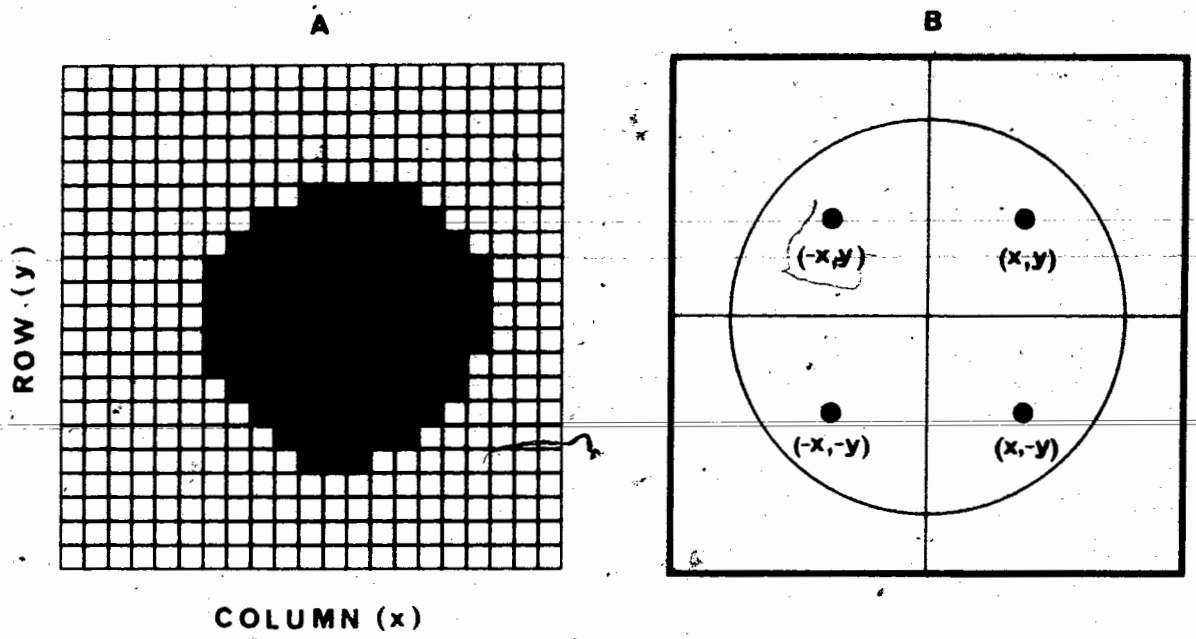
A
B
ROW (y)
COLUMN (x)
(-x,y)
(x,y)
(-x,-y)
(x,-y)

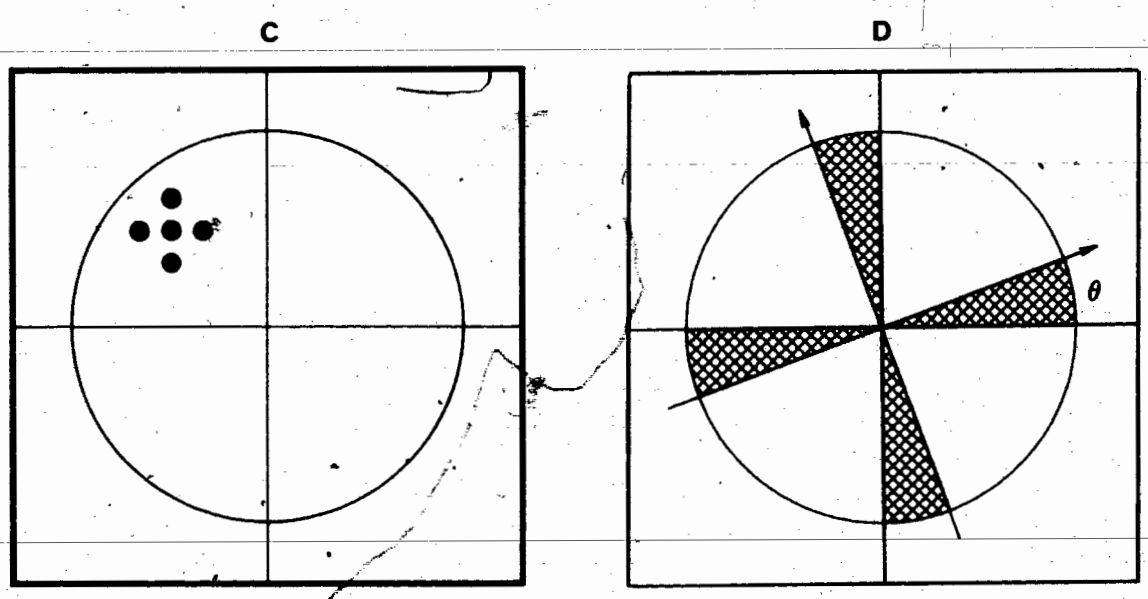
C
D
θ

otherwise assign it to quadrant 3.

After all points have been assigned to a particular quadrant QSI can then be calculated from the following:

$$QSI = 1/(q1/a)^2 + (q2/a)^2 + (q3/a)^2 + (q4/a)^2$$

Where q1 to q4 = the total area of the component in quadrant 1 to 4. and

a = the total area of the component being considered.

c. RING SYMMETRY INDEX

RSI attempts to estimate the local symmetry of a point by checking its nearest 8 neighbors. If we let 'n' be the total number of filled neighbors and 'a' be the total area of the component being considered then:

$$RSI = n/8a$$

This ratio is multiplied by 10 to force RSI to take on values between 0 (none of the 8 neighbors are of the same component) to 10 (all neighbors are of the same component).

d. CORE RATIO

CORAT provides an estimate of the cross-sectional contour of a cell nucleus by estimating the mean optical density of the nuclear perimeter (MODP) and comparing it

to the mean optical density of the central portion or core (MODC) of the image. CORAT is then calculated as the ratio of MODC:MODP. This ratio will be greater than 1 for any object that is not perfectly flat and homogeneous.

II. PROCESSING NUCLEAR IMAGES. (CELED)

Processing nuclear images is primarily concerned with removing above threshold but non-nuclear points from the digitized image. Once this has been done the image is considered to be clean. Cleaning nuclear images is usually done manually at a video-display terminal whereby a moving cursor is used to erase all extraneous background points from the image. The program that I am going to describe is capable of performing this task automatically.

Fig. 18A shows a raw image of a scan area which contains a nuclear image along with fragments of other nuclear images and a considerable amount of debris. The program has the task of recognizing what is part of the whole nuclear image and what is not.

CELED begins by assigning every above threshold point (the black regions) in the scan area a weight based on the number of nearest neighbors that are above threshold. 16 neighbors are examined. Those points with a weight of 6 are classified as background while those points with a weight greater than 9 are classified as image. Those points with a weight between 6 and 9 are examined more closely in order to increase or decrease their

weight. This is accomplished by first determining where the point is located relative to the nearest large object. that is, whether it is located on the right side, top, left side or bottom of the object.

When the location of the point has been established, an appropiate probe is invoked which examines 5 of the point's nearest neigbors. The weight of each point is recalculated and this weight is taken as the best estimate. The amount of cleaning that is possible with weight assignments is shown in Fig. 18B. We can see that it has removed nearly all of the scattered background points but that the larger images near the border still remain. This will always occur with large objects since the weights of their individual points will be within the image range.

Cleaning the scan area of large objects requires a different approach. Once the weight assignments have been complete the program begins to define the perimeter of every object that is left in the scan area by employing a set of vector probes (5 vectors/probe). CELED invokes a separate probe for the top,right side,bottom and left side of the the image. The probes move clockwise around the image and are set up in such a way as to enable the program to know when it has to switch from one probe to another. Although it is not essential, the probes are usually able to find their way back to the starting position after circumnavigating the object. These vectors are shown in Fig. 18C.

Once the perimeter of the object has been defined it is assigned a unique number. CELED then moves on to the next object and the process is repeated until all objects have been identified. After all objects have been examined the program not only knows how many objects are present, but it also knows the total area and circumference of each object. It then makes the assumption that the largest object is the one of interest and treats everything else as background. If the largest object lies on the border of the scan area it is deleted and the next largest object is treated as the image. The final image is then produced and is shown in Fig. 18D.

Figure 18. Algorithm for an automated procedure to clean digitized nuclear images.

A: Scan area before being cleaned of background

B: Scan area partially cleaned by weight assignments.

C: the four vector probes that are used to define the perimeter of all objects in the scan area.

D: the final cleaning stage, leaving only the nuclear image in the scan area.

A

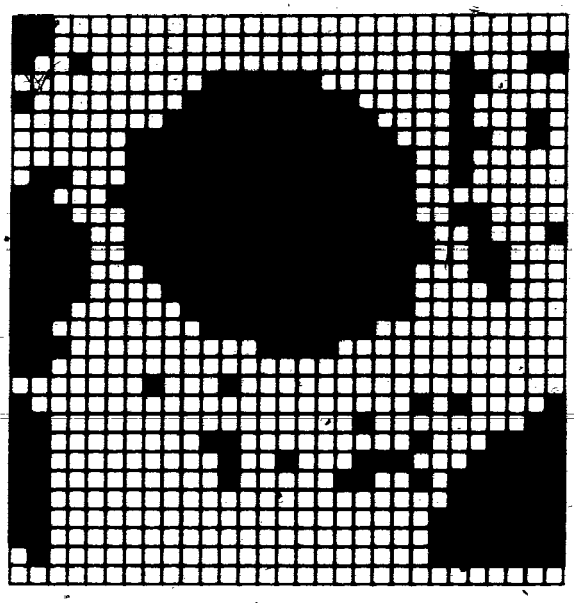

B

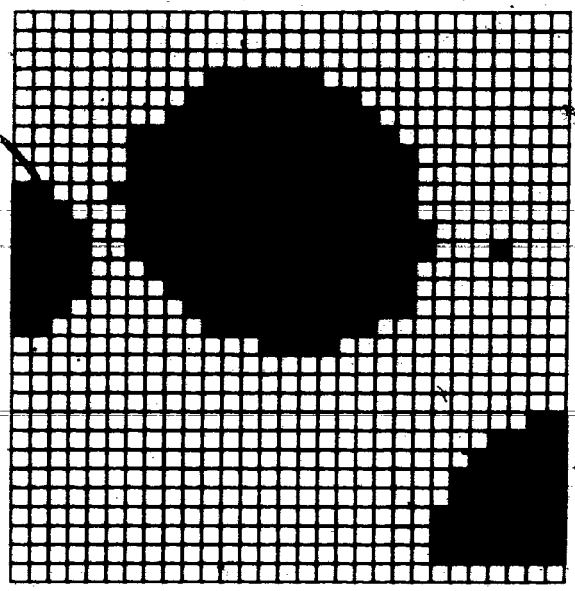

C

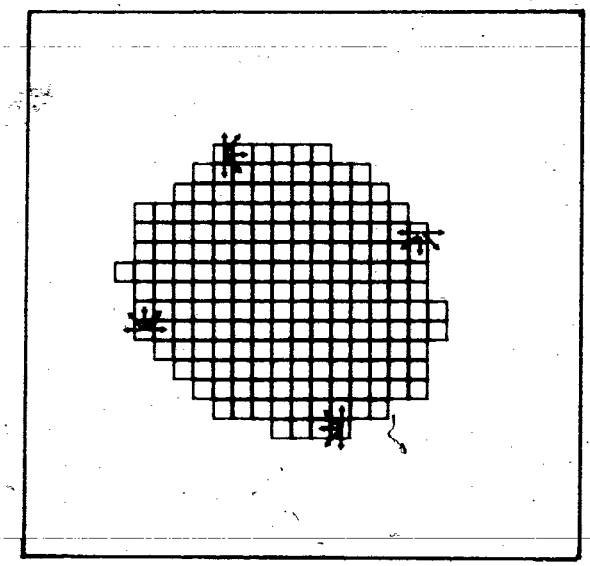

D

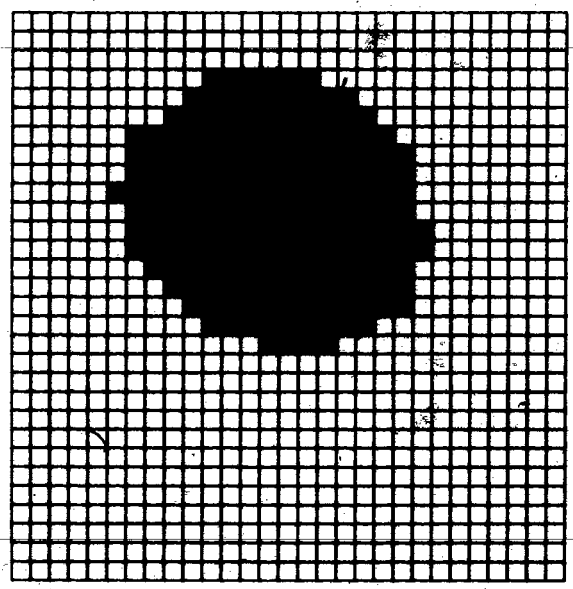

REFERENCES

Adams, T.S. and A.M. Hintz. 1969. Relationship of age, ovarian developement, and the corpus allatum to mating in the house-fly, Musca domestica. J. Insect Physiol. 15:210-215

Algeri, S., G. Calerni, G. Toffano and F. Ponzio. 1983. Neurotransmitter Alterations in aging rats. In: Aging of the Brain. ed. D. Samuel, Raven Press, N.Y. p 227-243

Ashburner, M. 1972. Patterns of puffing activity in the salivary gland chromosomes of Drosophila. Chromosoma (Berl) 38:255-281

Badr, E.A. 1972. Acid lability of nuclear DNA and its degree of binding to tritiated actinomycin D in meristematic and differentiated cells. Arch. Biol., 83:11-20

Bartels, P.H. 1979. Numerical evaluation of cytologic data III Selection of features for descrimination. Anal. Quant. Cytol., 1:153-159

Bedi,K.S. and D.J. Goldstein. 1978. Microdensitometric and autoradiographic comparison of DNA contents of feotal and adult rat liver nuclei. Histochem., 55:63-74

Brachet, J., H. Hulin and J. Guermont. 1968. Acid lability of DNA and cell differentiation. Exptl. Cell. Res., 51:509-518

Browder, L.W. 1980. Developmental Biology. Saunders college, Philadelphia. p. 158-170.

Brown, S.W. 1966. Heterochromatin. Science, 151:417-425

Clark, A.M. and M. Rockstein. 1964. Aging in insects. In: Physiology of Insecta, Vol II, Ch. 6. Acad. press, N.Y.

Collatz, K.G. and S. Collatz. 1981. Age dependent ultrastructural changes in different organs of the mecopteran fly Panorpa vulgaris. Exp. Geront., 16:183-193

Comings, D.E. and T.A. Okada. 1971. Condensation of chromosomes onto the nuclear membrane during prophase. Exp. Cell Res. 63:471-473

Daneholt, B. 1975. Transcription in poltene chromosomes. Cell 4:1-9

Davies, I., and A.P. Fotheringham. 1981. Lipofuscin: does it affect cellular performance? Exp. Gerontol., 16:119-125

Davies, J.E.W., P.M. Ellery and R. Hughes. 1977. Dietary ascorbic acid and life-span of guinea pigs. Exp. Geront., 12:215-216

Dilman, V.M. and V.N. Anisimov. 1979. Hypothalamic mechanisms of aging and of specific age pathology. Exp. Geront., 14:161-174

Edelmann, P. and J. Gallant. 1977. On the translational error theory of aging. Proc. Natl. Acad. Sci., 74:3396-3398

Enesco, H.E. 1967. A cytophotometric analysis of DNA content of rat nuclei in aging. J. Gerontol., 22: 445-448

Everitt, A.V. 1980. The neuroendocrine system and aging. Gerontology, 26:108-119

Fand, S. 1972. Environment conditions for optimal Feulgen hydrolysis. In: Introduction to Quantitative Cytochemistry-II, G.L.Wied and G.F.Bahr. (eds). p. 211-222 Acad. Press, N.Y.

Fankboner, M.D. 1978. A study of age-related changes in anterior midgut caecum epithelium of adult male Shistocerca gregaria (Forskal). M.Sc. Thesis, Simon Fraser University.

Felsenfeld, G. 1978. Chromatin. Nature, 271:115-121

Finch, C.E. 1973. Catecholamine metabolism in brains of aging mice. Brain Res., 52: 261-276

Finch, C.E. 1976. Physiological changes of aging in mammals. Quart. Rev. Biol., 51:49-83

Fleming, J.E., J. Miquel, S.F. Cottrel, L.S. Yengoyan and A.C. Economos. 1982. Is cell aging caused by respiration dependent injury in the mitochondrial genome? Gerontology, 28:242-244

Frenster, J.H., V. Allfrey, and A. Mirsky. 1963. Repressed and active chromatin isolated from interphase lymphocytes. Proc. Natl. Acad. Sci., 50:1026-1032

Gersh, I. 1973. Changing molecular patterns during cell maturation in the mouse. In: Submicroscopic Cytochemistry I Proteins and Nucleic Acids. I.Gersh, Ed. p. 251-268

Goldberg, A.C. and J.F. Dice. 1974. Intracellular Protein Degradation in Mammalian and Bacterial Cells. Ann. Rev. Biochem., 43:835-869

Hamkalo, B.A. and J.B. Rattner. 1980. Folding up genes and chromosomes. Quart. Rev. Biol., 55:409-417

Hancock, R. and M.E. Hughes. 1982. Organization of DNA in the interphase nucleus. Biol. Cell, 44:201-212

Harman, D. 1968. Free radical theory of aging: effects of free radical inhibitors on the mortality rate of LAF1 mice. J. Gerontol., 23:476-484

Harris, H. 1967. The reactivation of the red cell nucleus. J. Cell Sci., 2:23-32

Hothschild, R. 1971. Lysosomes, membranes and aging. Exp. Geront., 6:153

Hsu, T.T. 1962. Differential rate in RNA synthesis between euchromatin and heterochromatin. Exptl. Cell Res., 22:332

Igo-Kemenes, T. and H.G. Zachau. 1978. Domains in chromatin structure. Cold Spring Harbor Symp. Quant. Biol., 42:109-118

Jonec, V. and C.E. Finch. 1975. Aging and Dopamine uptake by subcellular fractions of the C57BL/6T male mouse brain. Brain Res., 91:197-215

Kiefer, R., G. Kiefer, S. Richard, R. Reinhard and W. Sandritter. 1973. A method for the quantitative evaluation of eu- and heterochromatin in interphase nuclei using cytophotometry and pattern analysis. Beitr. Path. Bd., 150:163-173

Kornberg, R.D. 1974. Chromatin stucture: a repeating unit of histones and DNA. Science, 184:865-868

Kozo, A., T.W. Borun and L.H. Cohen. 1981. Phosphorylation states of histone H1 subtypes and their relationship to chromatin functions during the HeLa S-3 cell cycle. Biochem., 20: 1445-1454

Lamb, J.B. 1977. Biology of aging. Halsted Press. p. 148.

Lamb, M.M. and B. Daneholt. 1979. Characterization of active transcription units in balbiani rings of Chironomus tentans. Cell, 17:835-848

Lapham, L.L. 1968. Tetraploid DNA content of purkenjie neurons of human cerebral cortex. Science, 159:310-312

Laibovitz, B.E. and B.V. Siegal. 1980. Aspects of free radical reactions in biological systems: aging. J. Gerontol., 35:41-56

Levenbook, L. and C.M. Williams. 1959. Mitochondria in the flight muscle of insects. J. Gen Physiol.,39:497-512

Littau, V.C., V.G. Allfrey, J.H. Frenster and A.E. Mirsky. 1964. Active and inactive regions of nuclear chromatin as revealed by electron microscope autoradiography. Proc. Natl. Acad. Sci., 52:93-100

Littau, V.C., C.J. Burdick, V.G. Allfrey and A.E. Mirsky. 1965. The role of histones in the maintenance of chromatin Structure. Proc. Nat. Acad. Sci., 54:1204-1212

Lyon, M.F. 1974. Gene and chromosome inactivation. Genetics, 78:305-309

Maclean, N. and V.A. Hilder. 1977. Mechanisms of chromatin activation and repression. Int. Rev. Cytol., 48:1-54

McGeer, P.L. and E.G. McGeer. 1981. Neurotransmitters in the aging brain. In: The Molecular Basis of Neuropathology. A.N. Davison and R.H.S. Thompson (ed). p. 631-648. Edward Arnold, Lond.

McKeon, F.D., D.L. Tuffanelli, S. Kobayashi and M.W. Kirschneri. 1984. The redistribution of a conserved nuclear envelope protein during the cell cycle suggests a pathway for

chromosome condensation. Cell, 36:83-92

Mello, M.L.S. 1978. Computer analysis of stained chromatin from the Malpighian tubes of Triatoma infestans (Klug Hemiptera Reduviidae). Mikroskopie Wien., 34:285-299

Mills, B.J. and C.A. Lang. 1976. The biosynthesis of DNA during the lifespan of the mosquito. Biochem. J. 154:481-490

Miller, A. 1965. The Internal anatomy and histology of the imago of Drosophila melanogaster. In: Biology of Drosophila. (ed). M. Demerec. Hafner, N.Y. p. 436

Miquel, J. 1971. Aging of male Drosophila melanogaster: Histological, Histochemical and Ultrastructural Changes. Adv. Geront. Res., 3:39-71

Miquel, J., R. Binnard, and J.E. Fleming. 1983. Role of metabolic rate and DNA-repair in Drosophila aging. Exp. Geront., 18:167-171

Monesi, V. 1965. Synthetic activities during spermatogensis of the mouse: RNA and protein. Exp. Cell Res., 39:197-224

Murvosh, C.M., R.L. Fye and G.C. LaBreque. 1964. Studies on the mating behavior of the house-fly, Musca domestica Ohio J. Sci., 64:264-271

O'Meara, A.R. and R.L. Herrmann. 1972. A modified mouse liver chromatin preparation displaying age-related differences in salt dissociation and template ability. Biochim. Biophys. Acta, 269:419-427

Orgel, L.E. 1963. The maintenance of the accuracy of protein synthesis and its relevance to aging. Proc. Natl. Acad. Sci., 49:517-521

Panar, L.C. and K.K. Nair. 1975. Cytochemistry of differentiating flight muscles of the desert locust Shistocerca gregaria. Histochem., 45:129-141

Pecile, A.E., E. Muller and G. Falconi. 1966. Endocrine function of pituitary transplants taken from rats of different ages. Arch. Int. Pharmacodyn. Ther., 159:434-441

Peng, M.T. and H.D. Huang. 1972. Aging of the hypothalamic-ovarian function in rat. Fertil. Steril., 23:535-542

Perreault, S.D., R.A. Wolf and B.R. Zirkin. 1984. The role of disulfide bond reduction during mammalian sperm nuclear decondensation in vivo. Dev. Biol., 101:160-167

Phytila, M. and F. Sherman. 1968. Age-associated studies on thermal stability and template effectiveness of DNA and nucleoproteins from beef thymus. Biochem. Biophys. Res. Comm., 31:340-344

Porter, K.R. and M.A. Bonneville. 1973. Fine structure of cells and tissues. Lea and Febizer, Philadelphia.

Renz, M., P. Nehls and J. Hozier. 1977. Involvement of histone H1 in the organization of the chromosome fiber. Proc. Nat. Acad. of Sci., 74:1879-1885

Rockstein, M. and H. Lieberman 1959. A Life table for the common fly Musca domestica. Gerontologia, 3:23-36

Rockstein, M. and K. Brandt. 1963. Enzyme changes in flight muscle correlated with aging and flight ability in the male housefly. Science, 139:1049-1052

Rockstein, M. and P.L. Bhatnagar. 1966. Duration and frequency of wing beat in the aging housefly, Musca domestica. Bio. Bull., Woods Hole. 131:479-486

Rockstein, M. and P.N. Srivastava. 1967. Trehalose in the flight muscle of the housefly, Musca domestica in relation to age. Experientia, 23:1-4

Rockstein, M. and W.B. Hawkins. 1970. Thiamine in the aging housefly, Musca domestica. Exp.Geront., 5:187-190

Rogers, R.E. and L.W. Browder. 1977. Characterization of RNA synthesis in cultered lampbrush-stage Rana pipiens oocytes. Dev. Biol., 55:148-159

Sherwood, E.M., P.H. Bartels and G.L. Wied. 1976. Feature selection in cell image analysis: use of the ROC curve. Acta Cytol., 20:254-260

Sohal, R.S., S.P. Sharma and E.F. Couch 1972. Fine structure of the neural sheath, glia and neurons in the brain of the housefly, Musca domestica. Z. Zellforsch, 135:449-459

Sohal, R.S. 1974. Fine structure of the Malpighian tubules in the Housefly, Musca domestica. Tissue and Cell, 6:719-728

Sohal, R.S. and H. Donato 1978. Effects of experimentally altered lifespans on the accumulation of fluorescent age pigments in the Housefly, Musca domestica. Exp. Geront., 13:335-341

Sohal, R.S. 1981. Relationship between metabolic rate, lipofuscin accumulation and lysosomal enzyme activity during aging in the adult housefly, Musca domestica. Exp. Geront., 16:347-555

Spelsberg, T.C., R.A. Webster and G.M. Pikler. 1976. Chromosomal proteins regulate steroid binding to chromatin. Nature, 262:65-67

Tas, S. 1978. Involvement of disulfide bonds in the condensed hetreochromatin and implications on cellular differentiation and aging. Gerontolgy, 24:358-364

Thoma, F., T.H. Koller and A. Klug. 1979. Involvement of histone H1 in the organization of the nucleosome and the salt-dependent superstructure of chromatin. J. Cell Biol., 83:403-421

Vidal, De Campos. B., G. Schluter and G.W. Moore. 1973. Cell Nucleus Pattern Recognition: Influence of Staining. Acta.

Cytologia, 17:510-515

Vogelstein, B., D.M. Purdoll and D.S. Coffey. 1980. Supercoiled loops and eucaryotic DNA replication. Cell, 22:79-85

von Hahn, H.P. 1970. Structural and functional changes in nucleoprotein during the ageing of the cell. Gerontologia, 16:116-128

Weinburg, G.H. and J.H. Schumaker. 1974. Statistics: an Intuitive Approach. Brooks/Cole pub. Monterey, Ca. p. 76-79

Weintraub, H. and M. Groudine. 1976. Chromosomal subunits in active genes have an altered conformation. Science, 193:848-856

Weisbrod, S. 1982. Active chromatin. Nature, 297:289-295

Weisbrod, S., M. Groudine and H. Weintraub. 1980. Interaction of HMG 14 and 17 with actively transcribed genes. Cell, 19:289-301

Wied, G.C., P.H. Bartels, G.F. Bahr and D.G. Oldfield. 1968. Taxonomic intercellular analytic system TICAS. for Cell Identification. Acta Cytol., 12:180-204

Wigglesworth, V.B. 1972. Insect Physiology. John Wiley and Sons. N.Y. p. 569-570

Wyllie, A.H., G.J. Beattie and A.D. Hargreaves. 1981. Chromatin changes in apotosis. Histochem. J., 13:681-692